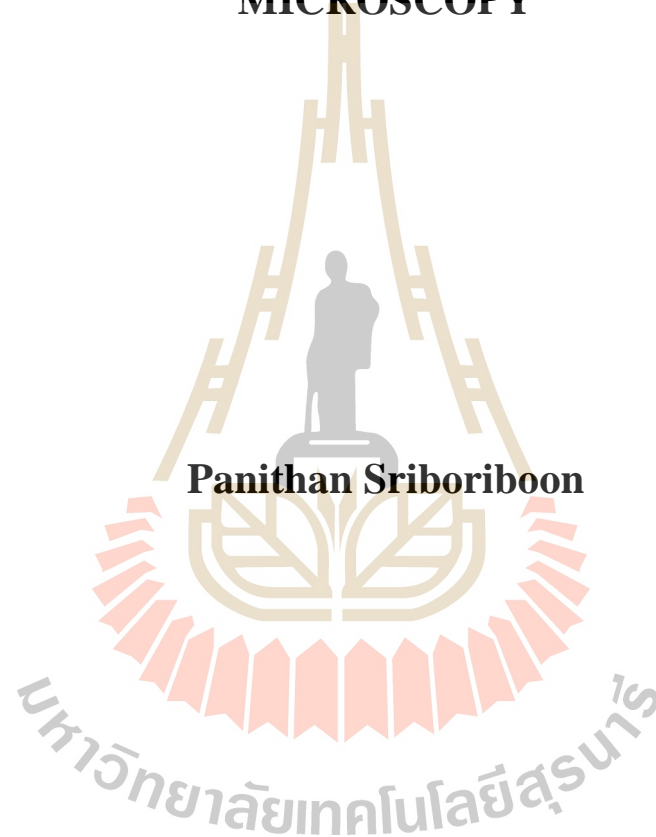


**PROPERTIES OF FERROELECTRIC DOMAINS OF  
BARIUM TITANATE AND BISMUTH FERRITE  
CERAMICS USING SCANNING PROBE  
MICROSCOPY**



**A Thesis Submitted in Partial Fulfillment of the Requirements for the  
Degree of Master of Science in Physics  
Suranaree University of Technology  
Academic Year 2018**

คุณสมบัติของเฟอร์โรอิเล็กทริกโดเมนของเซรามิกแบเรียมไททานเตและ  
บิสแมสเฟโรต์โดยใช้กล้องจุลทรรศน์แบบหัวสแกน



นายปณิธาน ศรีบริบูรณ์

วิทยานิพนธ์นี้เป็นส่วนหนึ่งของการศึกษาตามหลักสูตรปริญญาวิทยาศาสตรมหาบัณฑิต  
สาขาวิชาฟิสิกส์  
มหาวิทยาลัยเทคโนโลยีสุรนารี  
ปีการศึกษา 2561

**PROPERTIES OF FERROELECTRIC DOMAINS OF BARIUM  
TITANATE AND BISMUTH FERRITE CERAMICS USING  
SCANNING PROBE MICROSCOPY**

Suranaree University of Technology has approved this thesis submitted in partial fulfillment of the requirements for a Master's Degree.

Thesis Examining Committee

*N. Sanguansak*

(Dr. Nuanwan Sanguansak)

Chairperson

*Worason Kundhikanjana*

(Dr. Worason Kundhikanjana)

Member (Thesis Advisor)

*Wittawat Saenrang*

(Dr. Wittawat Saenrang)

Member

*Narong Chanlek*

(Dr. Narong Chanlek)

Member

*Santi Maensiri*

(Prof. Dr. Santi Maensiri)

Vice Rector for Academic Affairs  
and Internationalization

*Worawat Meevasana*

(Asst. Prof. Dr. Worawat Meevasana)

Dean of Institute of Science

ปณิธาน ศรีบริบูรณ์ : คุณสมบัติของเฟอร์โรอิเล็กทริกโดเมนของเซรามิกแบเรียมไททาเนต และบิสมัทเฟอไรต์โดยใช้กล้องจุลทรรศน์แบบหัวสแกน (PROPERTIES OF FERROELECTRIC DOMAINS OF BARIUM TITANATE AND BISMUTH FERRITE CERAMICS USING SCANNING PROBE MICROSCOPY) อาจารย์ที่ปรึกษา : อาจารย์ ดร.วรสุม กุญฑิกานจน์, 74 หน้า.

บิสมัทเฟอไรต์ ( $\text{BiFeO}_3$ ) เป็นวัสดุแม่เหล็กเฟอร์โรอิก (multiferroic) ที่ได้รับความสนใจอย่างมาก แต่สารส่วนใหญ่ที่ปลูกได้กลับมีการตอบสนองเชิงเพียโซต่ำ และกระแสรั่วไหลสูง เพราะมีสารอื่นเจือปน ทำให้ไม่สามารถนำไปใช้ในอุปกรณ์ได้จริง ในงานวิจัยนี้ศึกษาเฟอร์โรอิเล็กทริกโดเมนในแบเรียมไททาเนต ( $\text{BaTiO}_3$ ) และบิสมัทเฟอไรต์เจือซามาเรียม ( $\text{Bi}_{1-x}\text{Sm}_x\text{FeO}_3$ ) สำหรับแบเรียมไททาเนต งานวิจัยนี้ศึกษาการเปลี่ยนแปลงของการตอบสนองเชิงเพียโซของสารเมื่อเจือผงทองค่านาโนเพื่อศึกษาความเป็นไปได้ในการควบคุมทิศทางของโพลาริเซชันเมื่อสารตัวอย่างอยู่ในสนามไฟฟ้ากระแสตรงที่เหมาะสม สำหรับบิสมัทเฟอไรต์เจือซามาเรียม งานวิจัยนี้ศึกษาโครงสร้างผลึกรวม (polycrystalline) ของสารบิสมัทเฟอไรต์ ศึกษาสมบัติเฟอร์โรอิเล็กทริก และศึกษาการตอบสนองเชิงเพียโซ ที่เปลี่ยนแปลงไปเมื่อเจือด้วยซามาเรียม ซึ่งถูกเตรียม โดยวิธี simple co-precipitation  $\text{BiFeO}_3$  การศึกษาโครงสร้างใช้เทคนิค X-ray Diffraction (XRD) พบว่าเมื่อเจือ Sm จะทำให้สารเจือปน  $\text{Bi}_2\text{Fe}_4\text{O}_9$  ที่มีปะปนอยู่แล้วในตัวอย่าง  $\text{BiFeO}_3$  ลดลง แต่เมื่อเจือ Sm มากจนถึง Morphotropic Phase Boundary (MPB) ที่ 15% โครงสร้างของ  $\text{BiFeO}_3$  จะเปลี่ยนจาก Rhombohedral ( $R3c$ ) ไปเป็น Orthorhombic ( $Pnma$ ) การศึกษาโดเมนเฟอร์โรอิเล็กทริก และการนำไฟฟ้าของโดเมนเหล่านี้ การศึกษาโดยใช้กล้องจุลทรรศน์แบบส่องกราดชนิดวัดการตอบสนองเชิงเพียโซ (piezoresponse force microscopy) ทำให้เห็นโดเมนเฟอร์โรอิเล็กทริก โดยเฉลี่ยสารมีค่าการตอบสนองเชิงเพียโซที่มากขึ้นเมื่อเจือซามาเรียม แต่หายไปเมื่อเจือซามาเรียมถึง 15% เนื่องจากสารเปลี่ยนโครงสร้างที่ MBP ในขณะที่เคยกับพบว่า โดเมนเหล่านี้นำไฟฟ้า มีลักษณะ การนำไฟฟ้าเหมือนไดโอด โดยมีค่าการนำไฟฟ้าที่มากที่สุดเมื่อเจือ ซามาเรียมระหว่าง 0% ถึง 5%

สาขาวิชาฟิสิกส์  
ปีการศึกษา 2561

ลายมือชื่อนักศึกษา

ลายมือชื่ออาจารย์ที่ปรึกษา

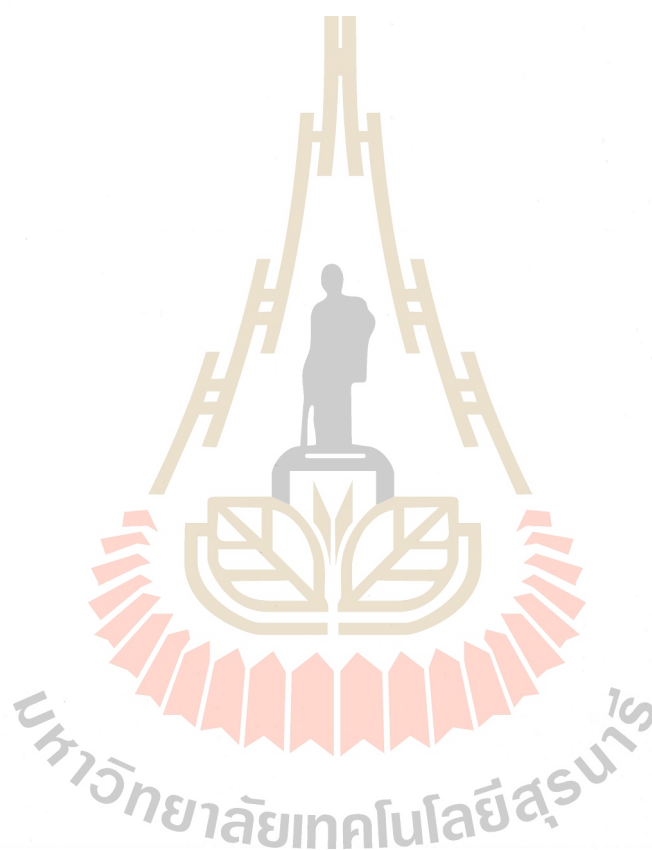


PANITHAN SRIBORIBOON : PROPERTIES OF FERROELECTRIC  
DOMAINS OF BARIUM TITANATE AND BISMUTH FERRITE  
CERAMICS USING SCANNING PROBE MICROSCOPY. THESIS  
ADVISOR : WORASOM KUNDHIKANJANA, Ph.D. 74 PP.

KEYWORDS: SCANNING PROBE MICROSCOPY, PIEZORESPONSE FORCE  
MICROSCOPY, CONDUCTIVE ATOMIC FORCE MICROSCOPY, FERROELECTRIC  
MATERIALS, BISMUTH FERRITE, BARIUM TITANATE

Bismuth ferrite (BFO) is one of the most studied and attractive multiferroic materials; however, low electrical polarization and sizable leakage current still prevents real device applications. In this project, we studied ferroelectric domains in barium titanate  $\text{BaTiO}_3$  (BT) and samarium (Sm) doped  $\text{BiFeO}_3$  (BFO),  $\text{Bi}_{1-x}\text{Sm}_x\text{FeO}_3$  ceramics. For the BT sample, we study change in PFM responses on Au-nanoparticles modified barium titanate as a function of DC voltage bias. The obtained results point towards possibility of control the polarization switching of the AuNPs-modified BT ceramics with fined-grains sizes, by a selection of the proper applied DC voltage ( $V_{dc}$ ). For BFO sample, the BFO samples were prepared by a simple co-precipitation method. The X-ray diffraction (XRD) patterns show that secondary phase,  $\text{Bi}_2\text{Fe}_4\text{O}_9$ , is suppressed when Sm doping amount is higher than 10%. A structural phase transition from rhombohedral (R3c) to orthorhombic phases (Pnma) at 15% Sm-doping was confirmed by XRD and Le Bail refinement. The Piezoresponse Force Microscopy (PFM) is used to acquire an image of polarization amplitude and phase of ferroelectric

domains. PFM images analysis demonstrated that average out of plane polarization amplitude increases as the Sm-substituted into the material before diminishing at doping 15% doping due to the phase transition at doping level 15%. Conductive AFM shows an average conductivity decreases at 7.5% doping, and I-V characteristics of the BFO domains shows diode behavior with similar ideality factor for different doping.



School of Physics

Academic Year 2018

Student's Signature



Advisor's Signature



## ACKNOWLEDGEMENT

I wish to thank my advisor Dr. Worasom Kundhikanjana for her endless patience, support, guidance, and advice provided over the course of my thesis. I would also like to thank the thesis examining committee, including Dr. Nuanwan Sanguansak, Asst. Dr. Wittawat Saenrang, and Dr. Narong Chanlek for their helpful and suggestions during my thesis defense. I would like to thank my family and my friends, Oradee Srikimkaew and Sartanee Suebka, for constant support throughout the learning process and encouragement.

I wish to thank Development and Promotion of Science and Technology Talents Project Scholarship Program, Thailand, and Center for Scientific and Technological Equipment (CSTE), Suranaree University of Technology (SUT). This project is supported by Thailand Research Fund (TRF) <http://www.trf.or.th/> (contract number TRG5880060), Suranaree University of Technology (SUT) [www.sut.ac.th](http://www.sut.ac.th), and (contract number SUT1-105-59-12-11 and SUT1-105-58-12-22), NANOTEC-SUT Center of Excellence on Advanced Functional Nanomaterial, and the Office of the Higher Education Commission under the National Research University (NRU) project.

Panithan Sriboriboon

# CONTENTS

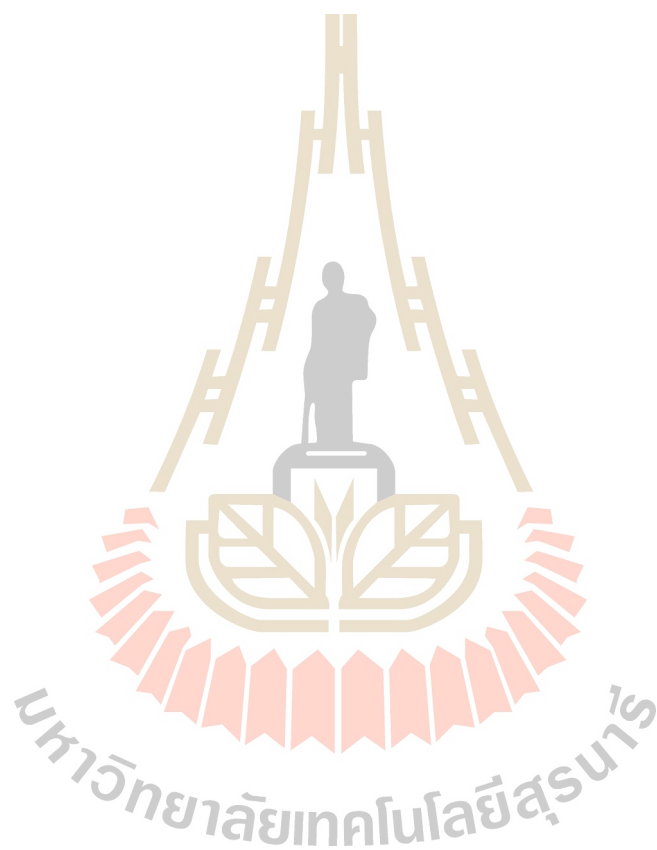
	<b>Page</b>
ABSTRACT IN THAI.....	I
ABSTRACT IN ENGLISH.....	II
ACKNOWLEDGEMENTS.....	IV
CONTENTS.....	V
LIST OF FIGURES.....	VIII
<b>CHAPTER</b>	
<b>I INTRODUCTION.....</b>	<b>1</b>
1.1 Ferroelectricity.....	1
1.2 Ferroelectric Materials.....	2
1.3 Nanoscale Ferroelectricity.....	4
1.4 Scanning Probe Microscopy for Nanoscale Ferroelectricity.....	5
1.5 Replaced Lead-Free Ferroelectric Materials.....	6
1.6 Barium Titanate.....	7
1.7 Bismuth Ferrite.....	8
1.8 Scope of This Thesis.....	9
<b>II LITERATURE REVIEWS.....</b>	<b>11</b>
2.1 PFM Investigation of Barium Titanate.....	11
2.2 Ferroelectricity in Bismuth Ferrite.....	13
2.3 Oxygen Vacancies in Bismuth Ferrite.....	14

## CONTENTS (Continued)

	<b>Page</b>
2.4 Temperature Induced Phase Transition of Bismuth Ferrite .....	15
2.5 Pressure Induced and Phase Transition of Bismuth Ferrite .....	15
2.6 Rare-Earth Substitution in Bismuth Ferrite.....	16
2.7 Ferroelectric Domain of Bismuth Ferrite.....	18
<b>III EXPERIMENTAL MEDTHODS.....</b>	<b>19</b>
3.1 Gold Nanoparticle-modified Barium Titanate (AuNPs-BT) .....	19
3.2 Sm-substituted Bismuth Ferrite (Sm-BFO) Samples.....	20
3.3 X-ray Diffraction Patterns of BFO Samples.....	20
3.4 BFO Grain Size Analysis.....	21
3.5 Piezoresponse Force Microscope Setup.....	22
3.6 Conductive Atomic Force Microscopy.....	25
3.7 Images Analysis and Statistical Methods.....	25
<b>IV RESULTS AND DISCUSSION.....</b>	<b>27</b>
4.1 Barium Titanate Study.....	27
4.2 PFM and C-AFM Studies of Sm-substituted BFO.....	33
4.3 Transport Properties of Sm-substituted BFO.....	40
<b>V CONCLUSIONS.....</b>	<b>44</b>
5.1 Sm-BFO Study.....	44
5.2 AuNPs-BT Study.....	45
5.3 Future Works.....	45

## CONTENTS (Continued)

	<b>Page</b>
REFERENCES.....	48
CURRICULUM VITAE.....	48



## LIST OF FIGURES

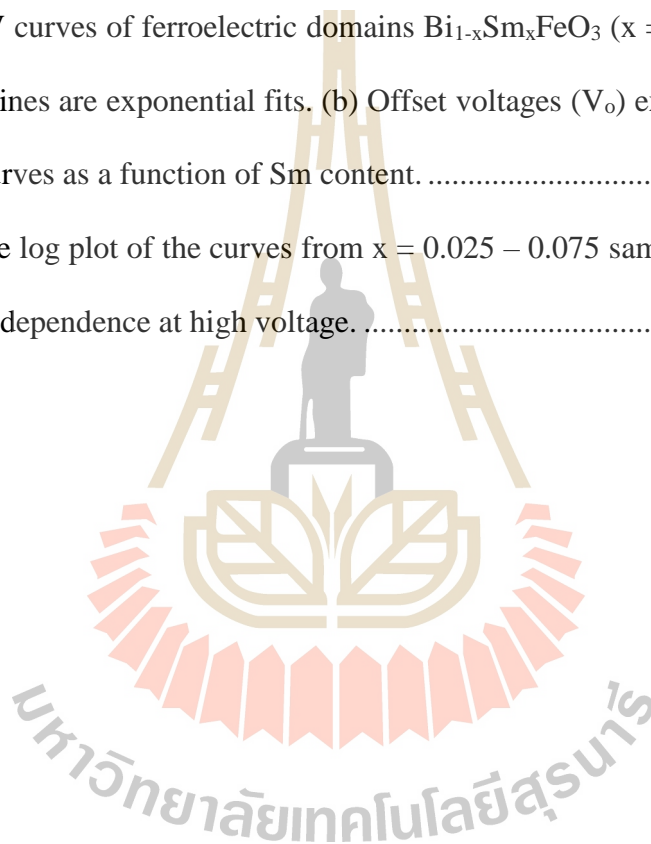
Figure	Page
1.1	Ferroelectric hysteresis loop ..... 1
3.1	Average grain size as a function of Sm-content. The square dot indicates the average grain size and the * are outliers.....21
3.2	(a) The XRD patterns of $\text{Bi}_{1-x}\text{Sm}_x\text{FeO}_3$ ( $x = 0, 0.025, 0.050, 0.075, 0.125, 0.150$ ) samples. * and $\times$ indicates $\text{Bi}_2\text{Fe}_4\text{O}_9$ and $\text{Bi}_2\text{O}_3$ phase, respectively. (b) Zoom in of Intensity peaks of the $\text{Bi}_2\text{Fe}_4\text{O}_9$ phase and $\text{Bi}_2\text{O}_3$ phase.....22
3.3	Piezoresponse force microscopy set up .....23
3.4	To obtain PFM calibration, we write up and down domain on calibration sample (PZT) by DC bias. PFM amplitude show magnitude of piezoresponse and PFM phase show domain up (bright) and down domain (Dark) .....24
3.5	PFM-Amplitude and PFM-Phase of Sm-5% BFO. Image acquired at DC bias = 0 -1 and +1 V ,which show piezoresponse and ferroelectric domain reversion due to external electrical field. ....25
4.1	Topographic images of BT ceramics with (a) 0.0%, (b) 2.0%, (c) 4.0% and (d) 8.0% of AuNPs sintered at $1250^\circ\text{C}$ for 2 h.....28
4.2	Amplitude (upper panel) and phase contrast (lower panel) PFM images of BT ceramics with (a) 0.0%, (b) 2.0%, (c) 4.0% and (d) 8.0% of AuNPs sintered at $1250^\circ\text{C}$ for 2 h.....31

## LIST OF FIGURES (Continued)

Figure	Page
4.3	PFM results of BFO sample from Sm 0 -12.5% .....34
4.4	Topography, PFM Amplitude, PFM Phase, and C-AFM images of $\text{Bi}_{1-x}\text{Sm}_x\text{FeO}_3$ ( $x = 0 - 0.150$ ) samples at various locations. The scale bars are $5 \mu\text{m}$ for the Sm 0% - 10%, 15% images, $1 \mu\text{m}$ for the Sm 12.5% images .....35
4.5	(a) - (d) Topography, (e)-(h) PFM Amplitude, (i) - (l) PFM Phase, and (m) - (p) C-AFM images of $\text{Bi}_{1-x}\text{Sm}_x\text{FeO}_3$ ( $x = 0, 0.050, 0.075, \text{ and } 0.125$ ) samples. The arrow points to the $1 \mu\text{m}$ particles located between the big grains. The white-dotted line indicates regions with zero response in both PFM and C-AFM channels. Red and white lines outline grains from the topography images with different PFM and C-AFM responses (see main text for details). The scale bar are $5 \mu\text{m}$ and $2.5 \mu\text{m}$ for the Sm 0% - 7.5% and Sm 12.5% images, accordingly. ....36
4.6	(a) – (b) average PFM response and average C-AFM signal as a function of Sm content for $\text{Bi}_{1-x}\text{Sm}_x\text{FeO}_3$ ( $x = 0 - 0.150$ ). For the average C-AFM signal, the regions excluding the non-conducting regions were used. The lines are guide to the eyes. (c) Areal fraction of the non-conducting region for $x = 0 - 0.075$ . ....37
4.7	Correlation of C-AFM, PFM phase, and PFM amplitude .....39
4.8	PFM and C-AFM images of Sm 0% and 5% samples taken at sample bias = 0, +10 V and -10 V .....39

## LIST OF FIGURES (Continued)

<b>Figure</b>		<b>Page</b>
4.9	Hysteresis loop in I-V characteristic.....	41
4.10	Tip bias I-V characterization .....	41
4.11	(a) I-V curves of ferroelectric domains $\text{Bi}_{1-x}\text{Sm}_x\text{FeO}_3$ ( $x = 0 - 0.075$ ). The solid lines are exponential fits. (b) Offset voltages ( $V_o$ ) extracted from the I-V curves as a function of Sm content. ....	42
4.12	Double log plot of the curves from $x = 0.025 - 0.075$ sample, which show linear dependence at high voltage. ....	43



# CHAPTER I

## INTRODUCTION

### 1.1 Ferroelectricity

Ferroelectricity is a characteristic of certain materials that have a spontaneous electric polarization that can be reversed by the application of an external electric field. All ferroelectrics are pyroelectric and some of them are piezoelectric, with the additional property that their natural electrical polarization is reversible. Ferroelectricity was discovered in 1920 in Rochelle salt by Valasek (Valasek, 1921). Thus, the prefix ferro, meaning iron, was used to describe the property regardless of the fact that most ferroelectric materials do not contain iron.

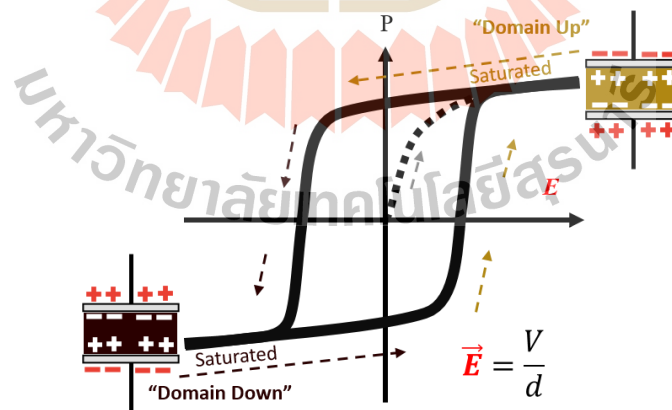


**Figure 1.1** Ferroelectric hysteresis loop.

When most materials are polarized, the polarization induced,  $P$ , is related to the applied external electric field  $E$ ; so the polarization is a linear function. This is called dielectric polarization (Figure 1.1). The electric permittivity, corresponding to the slope of the polarization curve, is not constant as in dielectrics but is a function of the external electric field. In addition to being nonlinear, ferroelectric materials demonstrate a spontaneous nonzero polarization, even when the applied field  $E$  is zero. The distinguishing feature of ferroelectrics is that the spontaneous polarization can be reversed by a suitably strong applied electric field in the opposite direction; the polarization is therefore dependent not only on the current electric field but also on its history, yielding a hysteresis loop. They are called ferroelectrics by analogy to ferromagnetic materials, which have spontaneous magnetization and exhibit similar hysteresis loops.

Typically, materials demonstrate ferroelectricity only below a certain phase transition temperature, called the Curie temperature ( $T_C$ ) and are paraelectric above this temperature: the spontaneous polarization vanishes, and the ferroelectric crystal transforms into the paraelectric state. Many ferroelectrics lose their piezoelectric properties above  $T_C$  completely, because their paraelectric phase has a centrosymmetric crystal structure (Safari and Akdogan, 2008).

## 1.2 Ferroelectric Materials

Ferroelectric materials have internal electric dipoles of a ferroelectric material are coupled to the material lattice so anything that changes the lattice will change the strength of the dipoles (in other words, a change in the spontaneous polarization). The change in the spontaneous polarization results in a change in the surface charge. This

can cause current flow in the case of a ferroelectric capacitor even without the presence of an external voltage across the capacitor. Two stimuli that will change the lattice dimensions of a material are force and temperature. The generation of a surface charge in response to the application of an external stress to a material is called piezoelectricity. A change in the spontaneous polarization of a material in response to a change in temperature is called pyroelectricity.

Generally, there are 230 space groups among which 32 crystalline classes can be found in crystals. There are 21 non-centro-symmetric classes, within which 20 are piezoelectric. Among the piezoelectric classes, 10 have a spontaneous electric polarization that varies with the temperature, therefore they are pyroelectric. Among pyroelectric materials, some of them are ferroelectric.

Ferroelectric phase transitions are often characterized as either displacive (such as  $\text{BaTiO}_3$ ) or order-disorder (such as  $\text{NaNbO}_3$ ), though often phase transitions will demonstrate elements of both behaviors. In barium titanate, a typical ferroelectric of the displacive type, the transition can be understood in terms of a polarization catastrophe, in which, if an ion is displaced from equilibrium slightly, the force from the local electric fields due to the ions in the crystal increases faster than the elastic-restoring forces. This leads to an asymmetrical shift in the equilibrium ion positions and hence to a permanent dipole moment. The ionic displacement in barium titanate concerns the relative position of the titanium ion within the oxygen octahedral cage. In lead titanate, another key ferroelectric material, although the structure is rather similar to barium titanate the driving force for ferroelectricity is more complex with interactions between the lead and oxygen ions also playing an important role. In an order-disorder ferroelectric, there is a dipole moment in each unit cell, but at high

temperatures they are pointing in random directions. Upon lowering the temperature and going through the phase transition, the dipoles order, all pointing in the same direction within a domain.

An important ferroelectric material for applications is lead zirconate titanate (PZT), which is part of the solid solution formed between ferroelectric lead titanate and anti-ferroelectric lead zirconate. Different compositions are used for different applications; for memory applications, PZT closer in composition to lead titanate is preferred, whereas piezoelectric applications make use of the diverging piezoelectric coefficients associated with the morphotropic phase boundary that is found close to the 50/50 composition. Ferroelectric crystals often show several transition temperatures and domain structure hysteresis, much as do ferromagnetic crystals. The nature of the phase transition in some ferroelectric crystals is still not well understood.

### **1.3 Nanoscale Ferroelectricity**

Ferroelectric materials exhibit a wide range of functional properties, including switchable polarization, piezoelectricity, high non-linear optical activity, pyroelectricity, and non-linear dielectric behavior. These properties are essential for application in electronic devices such as sensors, micro-actuators, infrared detectors, and, non-volatile memories (Dawber et al., 2005). Because of this unique combination of properties researchers and engineers have been focusing on ferroelectric materials for a long time. Several classical articles supported as an inclusive introduction into the field for a number of generations of scientists. However, modern developments in the synthesis and fabrication of micro and nanoscale ferroelectric structures brought to life new physical phenomena that need to be studied and understood at this scale. As

structure dimensions are getting smaller, ferroelectric materials show a noticeable size effect expressing itself in a significant unconventional properties of low-dimensional structures compared to the bulk properties. To understand the scaling behavior, several fundamental issues need to be addressed, including the intrinsic limit for a stable domain, extrinsic effects on polarization stability, mechanism of domain wall motion and switching in nanoscale volumes.

#### **1.4 Scanning Probe Microscopy for Nanoscale Ferroelectricity**

Progress in modern science is impossible without reliable tools for characterization of structural, physical, and chemical properties of materials and devices at the micro-, nano-, and atomic scale levels. While structural information can be obtained by such established techniques as scanning and transmission electron microscopy, high-resolution examination of local electronic structure, electric potential and chemical functionality is a much more daunting problem. Local electronic properties became accessible after the development of Scanning Tunneling Microscopy by G. Binnig and H. Rohrer in 1981 at IBM Zurich 25 years ago an invention that earned its authors the Nobel Prize in Physics five years later. Scanning Probe Microscopy (SPM) techniques are particularly useful for micro and nanoscale characterization of ferroelectric materials. SPM techniques have revolutionized the field of ferroelectricity, for providing an opportunity for nondestructive imaging of domain structures in ferroelectric thin films at the nanoscale. Among the SPM techniques for the nanoscale characterization of ferroelectrics, by far the most popular one is Piezoresponse Force Microscopy (PFM). Application of PFM, well known as critical role in the recent advances in science and technology of nanoscale ferroelectrics

(Gruverman and Kalinin, 2006). The PFM applied for high-resolution characterization of ferroelectrics domain wall (Tybell et al., 2002), nanoscale ferroelectric switching in inhomogeneous electrical and elastic fields (Gruverman et al., 2001), and mechanisms of ferroelectric fatigue (Shvartsman et al., 2005). Another importance is made on investigating the electrical and mechanical properties of ferroelectrics with a viewpoint of fabrication of nanoscale domain structures that can be used both for fundamental studies and for application related purposes (Terabe et al., 2003).

## 1.5 Replaced Lead-Free Ferroelectric Materials

Lead zirconate-titanate  $\text{Pb}(\text{Zr,Ti})\text{O}_3$  or PZT is the most widely used piezoceramic material for electromechanical device applications. The toxicity and environmental impacts of lead have been known, and many researchers has been finding lead-free alternatives (Jaffe, 2012). However, it was not until 2002 that directives regulating the use of Pb and other toxic elements in commercial products were introduced in the European Union (Directive, 2011, Directive, 2003). These regulations have stimulated renewed interest in lead-free piezoelectrics. In 2004 (Saito et al., 2004) reported alkaline-niobatebased lead-free piezoelectrics with properties comparable with those found in PZT. This report triggered an exponential increase in the number of both basic and applied research investigations related to lead-free piezoelectrics. The expanding research community soon revisited the pioneering work performed by Tadashi (Tadashi et al., 1991), which had reported on alkaline-bismuth-titanate-based piezoelectrics. Thereafter, research efforts focused on strategies to improve the piezoelectric properties of these materials. These strategies have included searching for systems with

morphotropic or polymorphic phase boundaries, microstructure optimization, and texturing.

## 1.6 Barium Titanate

BaTiO<sub>3</sub> (BT) was the early polycrystalline ceramic material ever learned that exhibited ferroelectricity. In the 1950s, it was considered a serious candidate for lead-free piezoelectrics transducer applications (Jaffe, 1950) and the basic phenomenological principle for the monodomain, monocrystalline state was established (Devonshire, 1949; 1951). Recently, great utilizations of lead-free ferroelectric ceramics particularly in the development of data storage devices for the next generation of information technology have been realized based on increasing sophisticated ferroelectric domain patterning. In connection with this, perovskite BT-based compounds are of particular interest as they are one of the most popular lead-free ferroelectric/piezoelectric materials employed in numerous existing commercial devices (Buscaglia et al., 2004; Fuentes et al., 2010; Tan et al., 2015).

Microstructural engineering is an effective strategy to tune functional properties of BT-based compounds. Gold nanoparticle (AuNPs)-modified BT ceramics which showed significantly almost 3-times-improved dielectric constant maxima and around 2-times-reduced dielectric loss values compared with unmodified BT ceramics, reported (Nonkumwong et al., 2015). Thus, the minor aim of this work is to explore domain evolution processes in polycrystalline BT-based ceramics containing various amounts of AuNPs. This is of significance because understanding the structure of these polarized BT-based ceramics and their polarization procedure is a fundamental necessity both for the development of novel materials and to improve their potential

device performance (Kim and Huber, 2015). Moreover, to date, no conclusive experimental data of such materials are available.

## 1.7 Bismuth Ferrite

$\text{BiFeO}_3$  (BFO) is a candidate for a lead-free piezoelectric material owing to its high remnant polarization, piezoelectric coefficient, and additional multiferroicity (Catalan and Scott, 2009). However, a large leakage current limits a number of BFO applications. Therefore, a number of studies report improved BFO properties by chemical substitutions either at A- or B- sites. Among these works, the A-site substitution with trivalent rare-earth elements with ionic radius smaller than Bi, such as  $\text{Sm}^{3+}$ ,  $\text{Gd}^{3+}$ ,  $\text{Dy}^{3+}$ , and  $\text{La}^{3+}$ , is of interests (Cheng et al., 2010; Fujino et al., 2008; Kan et al., 2011; V. A. Khomchenko et al., 2010; Walker et al., 2016; Yotburut et al., 2017; Yuan and Or, 2006). The chemical pressure from replacing Bi with a smaller atom causes structural transition from rhombohedral to orthorhombic with enhanced dielectric constant (Cheng et al., 2010), piezoelectric coefficient (Cheng et al., 2010; Fujino et al., 2008; Kan et al., 2010; Walker et al., 2016; Yotburut et al., 2017), and remnant magnetic polarization (Yuan and Or, 2006) at the phase boundary. This phase boundary is called morphotropic phase boundary similar what is found in lead-based ferroelectric materials (Lallart, 2011). Furthermore, the chemical substitutions also reduce the number of oxygen vacancies and  $\text{Fe}^{2+}$  ions, which are the major sources of leakage in BFO (Coondoo et al., 2012; Makhdoom et al., 2012; Mishra et al., 2008).

Recently, much attention is paid to transport behaviors at a metal-BFO interface, such as polarization-modulated rectifying behavior (Choi et al., 2009; Lee et al., 2011; Wang et al., 2011), photovoltaic effect (Choi et al., 2009; Paillard et al., 2016), and

ferroelectric resistive switching (Lee et al., 2011; Wang et al., 2011). These transport properties are greatly influenced by impurities and chemical defects (Kim et al., 2012; Yang et al., 2009); therefore, the properties should also change upon chemical substitutions. In this work, we study piezoresponse and transport property of ferroelectric domains in Sm-substitute BFO ceramics using piezoresponse force microscope (PFM) (Alikin et al., 2015; Soergel, 2011) and conductive atomic force microscope (C-AFM). These techniques allow direct measurements local piezoresponse, polarization direction, conductivity current-voltage (*I-V*) characteristic of the same ferroelectric domains (Choi et al., 2009; Lee et al., 2011; Paillard et al., 2016) to understand effects of chemical substitution and local polarization towards the transport properties.

### **1.8 Scope of This Thesis**

This research studies DC bias dependence of a gold nanoparticle modified barium titanate (AuNPs-BT) using PFM. This work is published in Integrated Ferroelectrics (Nonkumwong et al., 2018). This work addresses the domain evolution processes in polycrystalline barium titanate (BaTiO<sub>3</sub>, BT)-based ceramics containing various amounts of gold nanoparticles (AuNPs) as an additive by using piezoresponse force microscopy (PFM). This research study the polycrystalline BFO using scanning electron microscope (PFM) and conductive atomic force microscopy (C-AFM) spectroscopy. The PFM is used to determine the ferroelectric domain. X-ray diffraction (XRD) is used to characterize the structure of crystals and to analyze crystal structures. C-AFM is used to study the conductivity of a sample surface and a specific ferroelectric domain. Using PFM, C-AFM and XRD technique simultaneously to observe the

changes in electrical properties and polarization, which based on the crystalline structure of BFO.



## **CHAPTER II**

### **LITERATURE REVIEWS**

#### **2.1 PFM Investigation of Barium Titanate**

BT-based compounds are of particular interest as they are one of the most popular lead-free ferroelectric/piezoelectric materials employed in numerous existing commercial devices (Buscaglia et al., 2004; Fuentes et al., 2010; Tan et al., 2015). For most practical data storage applications, additive modified polycrystalline BT ceramics are more important than single crystal mainly because a good control over grain size and electrical characteristics can be obtained by tailoring the additive type and concentration, which lead to a wide range of applications (Rahaman and Manalert, 1998). In general, each area of the ferroelectric materials in which the spontaneous polarization points in one direction only, so-called “ferroelectric domain”, are separated by a domain wall (i.e. domain boundary) (Kao, 2004). Under static conditions, several techniques may be employed to visualize domain configurations of BT-based ceramics including optical (Cheng et al., 2006) and electron microscopy (Reichmann et al., 2011; Tan et al., 2015). One major source of the microscopic behavior of these ferroelectric ceramics for switching processes has been the use of neutron/X-ray/electron backscatter diffractions to indicate reorientation of the crystal lattice (Forrester et al., 2005; Park et al., 2007; Reichmann et al., 2011) individual domains of such materials. Previously, etching in conjunction with a standard optical microscope is a typical approach to obtain an image of the domain structure and can be accomplished in any laboratory without

the requirement of any specific facilities. Although, the use of optical microscopy to observe large domains in ferroelectrics is well-known, but this technique is unsuitable for the submicron domains found in fine-grained and opaque BT-based ceramics (Kim and Huber, 2015).

On the other hand, since the PFM was introduced by Güthner and Dransfeld in 1992 (Güthner and Dransfeld, 1992), this technique has become a promising approach for revealing ferroelectric domain patterns with a high lateral resolution of about 10 nm and has also proven to be extremely sensitive as it allows measurement of local surface displacements in the sub-pm regime (Jungk et al., 2010). Moreover, taking the advantage of the fact that ferroelectricity entails piezoelectricity, the domain pattern can be visualized by its piezo-mechanical deformation under the application of an electric field. In the case of PFM, the electric field is applied locally to the sample with the help of the tip (Soergel, 2011). Owing to its versatile, easy-to-handle, non-invasive technique for imaging ferroelectric domain patterns on any kind of ferroelectric material without the need of an elaborate sample preparation, PFM technique has been attracting growing attention (Kim and Huber, 2015; Soergel, 2011). To the best of our knowledge, no attempt has been made to use PFM technique to investigate domain patterns and also domain growth of AuNPs-modified BT ceramics which showed significantly almost 3-times-improved dielectric constant maxima and around 2-times-reduced dielectric loss values compared with unmodified BT ceramics, reported in our previous work (Nonkumwong et al., 2015). Thus, the aim of this work is to explore domain evolution processes in polycrystalline BT-based ceramics containing various amounts of AuNPs. This is of significance because understanding the structure of these polarized BT-based ceramics and their polarization procedure is a fundamental

necessity both for the development of novel materials and to improve their potential device performance (Kim and Huber, 2015). Moreover, to date, no conclusive experimental data of such materials are available.

## 2.2 Ferroelectricity in Bismuth Ferrite

Bismuth ferrite,  $\text{BiFeO}_3$  (BFO), is multiferroic materials with high transition temperature,  $T_N \sim 370\text{C}$ ,  $T_C \sim 830\text{C}$ . Due to the high transition temperature application refer to an application of multiferroic is possible at room temperature, so many researchers was attracted to study multiferroic properties of BFO (Eerenstein et al., 2006). The structure of BFO at room temperature is rhombohedral (space group  $R3c$ ) and polarization axis is along with the  $[111]_{\text{presudocubic}}$  axis (Moreau et al., 1971). Consider the atom in rhombohedral structure, Oxygen is pressed by surrounding atom, and not stable (Goldschmidt, 1926). Therefore, it rotated around the axis  $[111]_{\text{presudocubic}}$  cause the Fe-O-Fe bending angle estimate 154-156 degree (Moreau et al., 1971). This little rotating angle allows superimpose of Fe-O orbital, which indicate the antiferromagnetic properties. Although, BFO is being antiferromagnetic but it is paraelectric, which is not practical for application. However, turning BFO into ferroelectric and antiferromagnetic was engaged by Spaldin's hypothesis (Filippetti and Hill, 2002), which is suggest the transition-metal oxide with perovskite structure ( $\text{ABO}_3$ ), such as BFO, can be turn into ferroelectric and antiferromagnetic by ion-substitution at B site. This hypothesis emerge research field that develop the perovskite ( $\text{ABO}_3$ ) oxide material as multiferroic materials.

In polycrystalline BFO, primary phase, rhombohedral (space group  $R3c$ ) yielded high polarization (Diéguez et al., 2011), is indicated multiferroic properties of the

sample but the sample is naturally tended to contain other phases, such as  $\text{BiFe}_4\text{O}_9$ , and oxygen vacancy (Uchida et al., 2006). Polycrystalline sample must be purified by removing the oxygen vacancy and impurity phase  $\text{BiFe}_4\text{O}_9$ , therefore the idea of doping ion to improve multiferroic efficiency was reported (Hu et al., 2009; Yan et al., 2010). Recently, doping rare earth materials in BFO is seen to be a multi-purpose. For example, doping rare earths consequently fill the oxygen vacancy to lower the leakage current (Das et al., 2012; Vanga et al., 2015), reduce impurity phase, turn BFO from paraelectric into ferroelectric (Nalwa et al., 2008), and left the remnant electrical polarization in sample surface (Lebeugle et al., 2007; Lobo et al., 2007; Uchida et al., 2006).

### **2.3 Oxygen Vacancies in Bismuth Ferrite**

Bismuth ferrite synthesized in bulk and thin film form both have antiferromagnetic, ferroelectric and piezoelectric properties. Bismuth ferrite is not a naturally occurring and several synthesis methods have been developed. The wet chemical synthesis methods based on sol-gel chemistry synthesis have been used to make  $\text{BiFeO}_3$ . The advantage of this method is the compositional homogeneity of the precursors and the much lower calcined temperatures needed, which provide reduced impurity of bismuth. A precursor is calcined at 300-600°C to remove organic residuals and to promote crystallization of the bismuth ferrite perovskite phase, while the disadvantage is that the resulting powder must be sintered at high temperature to make a dense polycrystalline. The problem of synthesizing single phase BFO is the remaining of oxygen vacancies after synthesized. To reduce oxygen vacancies, the substitutions of rare-earth in BFO also helped. Since, Sm substitution not only improve the electrical

properties but also improved the ferroelectric behavior. In addition, the bond dissociation energy of Sm-O bond ( $619\pm 13$  kJ mol<sup>-1</sup>) being higher than of Bi-O bond ( $343\pm 6$  kJ mol<sup>-1</sup>), so Sm substitution for using Bi<sup>3+</sup> will recover the oxygen. Thus, it can be predictable that A-site substituted BFO samples will exhibit better ferroelectric, improve the electrical properties, and reduce oxygen vacancies.

## 2.4 Temperature Induced Phase Transition of Bismuth Ferrite

Bismuth Ferrite (BFO) is synthesized from two precursor Bi<sub>2</sub>O<sub>3</sub> and Fe<sub>2</sub>O<sub>3</sub> in the equal ratio. Phase transition from  $\alpha$ -Phase (ferroelectric) to  $\beta$ -Phase (paraelectric) occur at 825°C. Filippetti and Hill study BFO synthesis at difference temperature. They reported that the yield trendy have high impurity phase (parasitic phases or secondary phases) such as BiFe<sub>4</sub>O<sub>9</sub> or Bi<sub>2</sub>Fe<sub>4</sub>O<sub>9</sub>. These impurity are change the transition temperature and also effect the ferroelectric properties of bismuth ferrite (Filippetti and Hill, 2002).

## 2.5 Pressure Induced and Phase Transition of Bismuth Ferrite

Pashkin report phase transition of bismuth ferrite from pressure, 7.5-10 GPa at room temperature (Pashkin et al., 2007). From the experimental, pressure induced phase transition occur at about 10 GPa and the structure change from Rhombohedral (R3c) to Orthorhombic-Pnma (Pbnm). Afterward, Palai (Palai et al., 2007) propose that the phase transition from  $\alpha$ -Phase (ferroelectric) to  $\beta$ -Phase (paraelectric) occur at 825°C. However, this proposal is not accept until Redfern confirm the transition at 10GPa by the experiment (Redfern et al., 2009).

Another way similarly with pressure induced is metal doping, substitution of atom in structure with equal ion but difference atomic size. This method called a chemical pressure. For example,  $\text{La}^{3+}$  substitute  $\text{Bi}^{3+}$  in  $\text{BiFeO}_3$ . La and Bi size is not significantly difference but lone pair electron of La is not equal with Bi, so it consequently turn off Bi lone pair electron and also turn off ferroelectric properties (Polomska et al., 1974).

## 2.6 Rare-Earth Substitution in Bismuth Ferrite

Many group of researchers modify bismuth ferrite to show ferroelectricity. In 1969, Smolenskii's group (Smolenskii and Kraĭnik, 1969) report that bismuth ferrite is not purified, conductive and not practical with applications. However, the conductivity is caused by oxygen vacancy and iron ion. After that, the new research is set to the elimination of the oxygen vacancies and reduction of conductivity.

Recently, much attention is pay to the enhancement of bismuth ferrite. For example, Ramesh's group in 2003 report BFO with very high Remnant Polarization (Pr), 15 times better than founded before (Wang et al., 2003), and also have better ferromagnetism (1.0 Bohr magneton per unite cell). In 2006-2007, many research report a successful synthesis methods, which obtain polycrystalline BFO with high intrinsic polarization and almost zero intrinsic magnetization (Cazayous et al., 2007; Lebeugle et al., 2007; Lobo et al., 2007).

Rare-earth substitution at A-site of  $\text{ABO}_3$  of bismuth ferrite cause the transition of unit cell structure. Smaller atomic size will cause distortion and influence the ferroelectric and piezoresponse. However, the rare-earth doping also cause impurity phase such as  $\text{BiFe}_4\text{O}_9$  and also form new structure which is not  $\text{ABO}_3$  form. For

example, Uchida (Uchida et al., 2006) study La and Nd substituted bismuth ferrite, which not only improve piezoresponse but also form impurity phase.

Dieguez (Diéguez et al., 2011) used first principle calculation to predict all possible structure of bismuth ferrite when doped with Samarium and calculate piezoresponse coefficient. They report each possible structure have difference piezoresponse. For example, piezoresponse of space group  $R3c$  is  $90 \text{ C/m}^2$  and space group  $Pnma$  is  $0 \text{ C/m}^2$ . This results indicate that impurity phase effect the piezoresponse of polycrystalline.

Doping content of rare-earth is influent the structure possible structure of Bi, Fe and O. For example, the research of Khomchenko (V. Khomchenko et al., 2010) reported an effect of Dysprosium (Dy) doping in bismuth ferrite and at 20% content the structure rhombohedral ( $R3c$ ) changed into orthorhombic ( $Pnma$ ). This is called the morphological phase transition.

Nalwa (Nalwa et al., 2008) study synthesis of BFO, focusing on the multiferroic properties of as a function of samarium (Sm) doping content. The synthesis of Sm-BFO is used the Solid-state-reaction with the precursor,  $\text{Fe}_2\text{O}_3$ ,  $\text{Bi}_3\text{O}_3$  and  $\text{Sm}_2\text{O}_3$ . Temperature used in calcination is vary from in order to eliminate inessential organic compound. From the experimental found that calcination BFO at  $850^\circ\text{C}$  and Sm-BFO at  $800^\circ\text{C}$  for 1h can obtain the pure phase BFO without impurity, characterized by XRD.

Finally, the rare-earth substitution at Bi or Fe site helps to relief the conductivity, the loss factor, and also enhances the ferroelectric polarization is confirmed (Jun et al., 2005; Qi et al., 2005),. The rare earth doping is induced the structure transition and also confirm as a universal properties (Kan et al., 2010b) called a morphotropic phase

boundary (MPB), which large piezoresponse and related electrical properties are observed near this point.

## 2.7 Ferroelectric Domain of Bismuth Ferrite

Polarization direction of bismuth ferrite is pointing along the diagonal of pseudocubic (Polarization along  $[111]_{\text{pseudocubic}}$  axis), which have 8 possible directions. However, they are 3 directions  $71^\circ$ ,  $109^\circ$ ,  $180^\circ$ , respect to the domain walls that separate between two domains. Ferroelectric domain size is depend on thin film thickness, also ferroelectric (Mitsui and Furuichi, 1953) ferroelastic (Zheng et al., 2004) and multiferroic (Daraktchiev et al., 2008). Domain size is depended on a competition of strain, depolarization, and demagnetization, which effect the domain wall. Domain wall energy is a ratio between domain size and film thickness. The interesting relation of domain wall size ( $w$ ) and film thickness ( $d$ ) is  $w = A\sqrt{d}$ , where  $A$  is the constant (Chen et al., 2007). These works show that the thickness of sample indicate ferroelectric properties, however this work study bulk properties, which the thickness is not affect the results.

## CHAPTER III

### EXPERIMENTAL MEDTHODS

#### 3.1 Gold Nanoparticle-modified Barium Titanate (AuNPs-BT)

Jeeranan Nonkumwong from Chiang Mai University provided the BaTiO<sub>3</sub> for this research, which synthesized by employing a mixed-oxide synthetic route (Nonkumwong et al., 2014). Starting precursors were commercially available powders of BaCO<sub>3</sub> and TiO<sub>2</sub> (Aldrich, 99% purity). The method of mixing, drying and grinding of the products was similar to those employed in the earlier work (Nonkumwong et al., 2014). The mixed powders were vibro-milled (McCrone Micronizing Mill) for 0.5 h in ethyl alcohol, dried at 120°C and calcined at 1300°C for 2h. The citrate reduction method was used to prepare 50 nm gold nanoparticles (AuNPs). Briefly, aliquot of 0.16 ml of 1% w/v C<sub>6</sub>H<sub>5</sub>Na<sub>3</sub>O<sub>7</sub> (Aldrich, 99% purity) was added into the boiled HAuCl<sub>4</sub> solution which composed of 1.00 ml of 1% w/v HAuCl<sub>4</sub> (Strem Chemicals Co., 99% purity) and 50 ml of deionized water. After boiling for 15 min, purple-brown AuNPs solution was obtained. The AuNPs were purified via centrifugation method and washed with deionized water. Instead of using only 0.5% AuNPs, various amounts of AuNPs ranging from 0.0 to 4.0% were mixed with calcined BT powders via a rapid vibro-milling for 10 min without grinding media. Ceramics fabrication was successfully performed without any binders by uniaxial pressing of all compositions into green

pellets (15 mm in diameter) at 100 MPa and then sintered in a closed alumina crucible at 1250°C for 2 h with heating/cooling rates of 5°C/min.

### 3.2 Sm-substituted Bismuth Ferrite (Sm-BFO) Samples

Samples are provided by Yotburut (Yotburut et al., 2017). Nanoparticles of  $\text{Bi}_{1-x}\text{Sm}_x\text{FeO}_3$  with  $x = 0, 0.05, 0.1, 0.2,$  and  $0.3$  (abbreviated as BFO, BLFO-0.05, BLFO-0.1, BLFO-0.2, and BLFO-0.3, respectively) were prepared by a simple coprecipitation method. In this method, the raw materials used high purity chemical reagents (>99%)  $\text{Bi}(\text{NO}_3)_2 \cdot 5\text{H}_2\text{O}$ ,  $\text{Fe}(\text{NO}_3)_2 \cdot 9\text{H}_2\text{O}$ , and  $\text{Sm}(\text{NO}_3)_3 \cdot 4\text{H}_2\text{O}$  according to the stoichiometric ratio. For the initial step, the metal nitrates were mixed in deionized water at room temperature into the ready precursor solution. Second, the nitric acid and PEG were subsequently added to the solution with constant stirring and then increased the temperature to 60°C to form gel. Next, the ammonia solution was added into the above mixture until the precipitation was complete, and the solution was washed by deionized water for 5-6 times in order to remove the excess amine groups. The resulting mixture was dehydrated in an oven at 70°C. The dried  $\text{Bi}_{1-x}\text{Sm}_x\text{FeO}_3$  precursors were calcined in air at 600°C for 3 h and then were ground. Finally, the ground powders were pressed into pellets of 10 mm diameter applying pressure of 200 MPa and sintered at 800°C for 3 hours in air.

### 3.3 X-ray Diffraction Patterns of BFO Samples

The XRD patterns of polycrystalline  $\text{Bi}_{1-x}\text{Sm}_x\text{FeO}_3$  are showing in Figure 3.2(a). Pure BFO ( $x=0$ , or Sm 0%) structure is identified as rhombohedral (space group  $R3c$ ) and also have a small amount of impurity phase  $\text{Bi}_2\text{Fe}_4\text{O}_9$  (space group  $Pbnm$ )

mixed in the polycrystalline. The Sm substitutes on A-site of BFO, shown by shifting of the XRD peaks, see Figure 3.2(b). Sm substitution has two effects on the polycrystalline. First, the amount of secondary phase  $\text{Bi}_2\text{Fe}_4\text{O}_9$  and  $\text{Bi}_2\text{O}_3$  observed at  $2\theta \approx 28^\circ$  are reduced after Sm content increased. Almost pure polycrystalline of orthorhombic are observed at  $x = 0.10$  (Sm 10%) and  $x = 0.125$  (Sm 12.5%). Second, the Le Bail refinement show that cell parameters and cell volume of the rhombohedral structure are decreased as a function of Sm content. The morphotropic phase boundary (MBP) and phase transition from rhombohedral (space group  $R3c$ ) into orthorhombic (space group  $Pnma$ ) is observed at  $x = 0.15$  (Sm 15%).

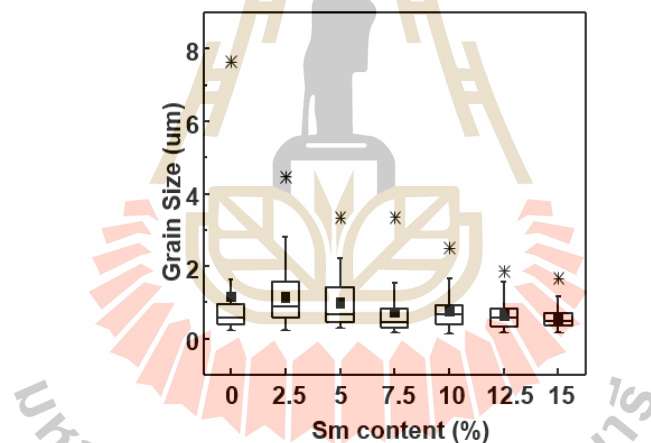


**Figure 3.1** Average grain size as a function of Sm-content. The square dot indicates the average grain size and the \* are outliers.

### 3.4 BFO Grain Size Analysis

Average grain size is using the Topography image from PFM to measure cross average section of grain using ImageJ software. The images using to for grain size analysis are 5-10 images for each doping and the results are showing in Figure 3.1.

### 3.5 Piezoresponse Force Microscope Setup

The working principle of PFM is based on the atomic force microscopy, which use a cantilever scan on sample surface for image acquisition. PFM required conductive cantilever to apply external AC signal from function generator to the cantilever tip to stimulate piezoresponse (Figure 3.3). This AC frequency is used as an operation frequency for as well as reference frequency to detect piezoresponse vibration for lock-in amplifier. Detection of a local piezoresponse vibration signal generated by the converse piezoelectric effect when an external DC voltage is applied between the PFM tip and the sample bottom electrode. The amplitude and phase signals of PFM are directly related to the Out of Plane amplitude of the effective piezoelectric coefficient and the polarization orientation, respectively.

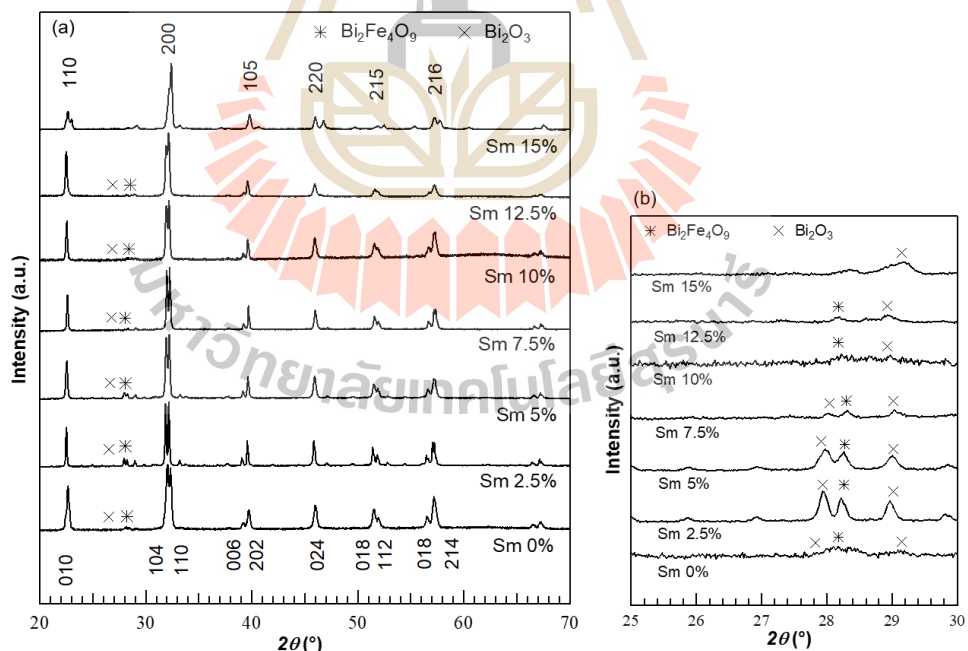


**Figure 3.2** (a) The XRD patterns of  $\text{Bi}_{1-x}\text{Sm}_x\text{FeO}_3$  ( $x = 0, 0.025, 0.050, 0.075, 0.125, 0.150$ ) samples. \* and x indicates  $\text{Bi}_2\text{Fe}_4\text{O}_9$  and  $\text{Bi}_2\text{O}_3$  phase, respectively. (b) Zoom in of Intensity peaks of the  $\text{Bi}_2\text{Fe}_4\text{O}_9$  phase and  $\text{Bi}_2\text{O}_3$  phase.

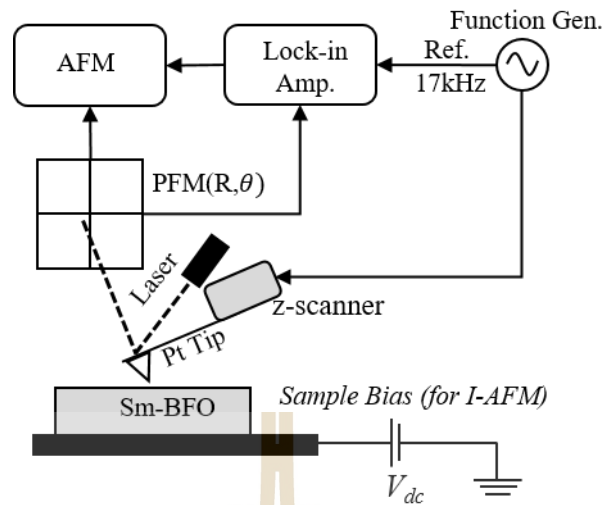


**Figure 3.3** Piezoresponse force microscopy set up.

The piezoresponse were imaged by commercial Piezoresponse Force Microscopy (PFM), Park AFM (model XE-120). The PFM operated in contact mode of Atomic Force Microscopy (AFM). In this case, we particularly study the vertical polarization of polycrystalline, the lateral polarization components are certainly non-zero and embedded as the spatial resolution of PFM images. The PFM cantilever is commercial Platinum (Pt) cantilever (25Pt200B-H). The cantilever spring constant is 250 N/m and the resonance frequency is 100 kHz, far from the reference frequency. SR-830 Lock-in Amplifier was using as data acquisitions and feed data back to AFM controller as PFM amplitude and phase. The lock-in Amplifier have reference frequency at 17 kHz, amplitude 2.5 V<sub>pp</sub> from function generator, Keysight33210A. Average piezoresponse value from the images was done by XEI, the commercial image processing software from Park AFM. Conductivity probe AFM or C-AFM, were performed using the same Pt tip, and scan rate were 0.5 Hz. I-V spectroscopy data acquired by C-AFM is characterized the diode effect using MATLAB. All scanning probe measurements were performed in the ambient environment at room temperature Images data from PFM are

Topography, PFM amplitude, and PFM phase. PFM calibration, PFM image of PZT with out of plane domain, up and down domain, is showing in Figure 3.4. The PFM amplitude show magnitude of piezoresponse and PFM phase show the polarization direction  $-180^\circ$  (bright) and  $180^\circ$  (dark) is up and down domain, respectively.

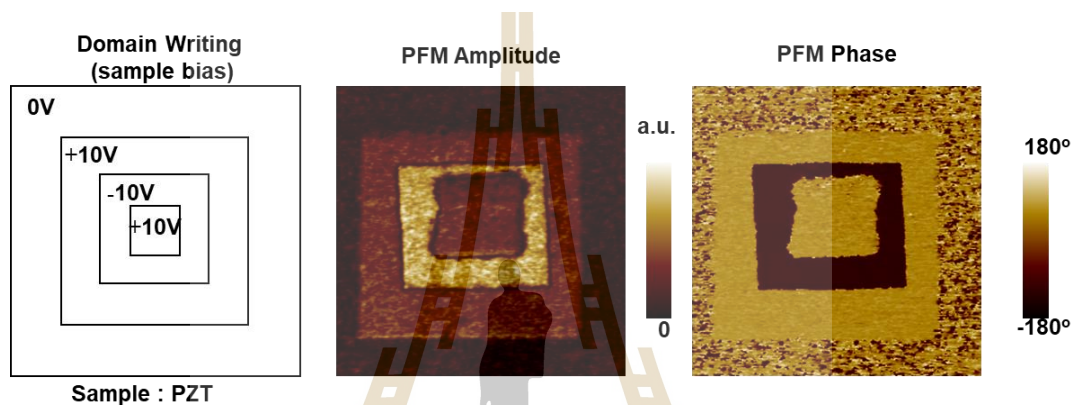


**Figure 3.4** To obtain PFM calibration, we write up and down domain on calibration sample (PZT) by DC bias. PFM amplitude show magnitude of piezoresponse and PFM phase show domain up (bright) and down domain (dark).

Figure 3.5 is the PFM image of Sm 5% BFO. On the surface, the polarized domain in out of plane extend in out of plan with  $\Delta z = d_{33}|V_{ac}|$ , (Kalinin et al., 2006). This expanding is acquired in PFM amplitude and PFM phase. PFM amplitude is refer to the piezoelectric coefficient, while PFM phase show the polarization direction respect to the plane.

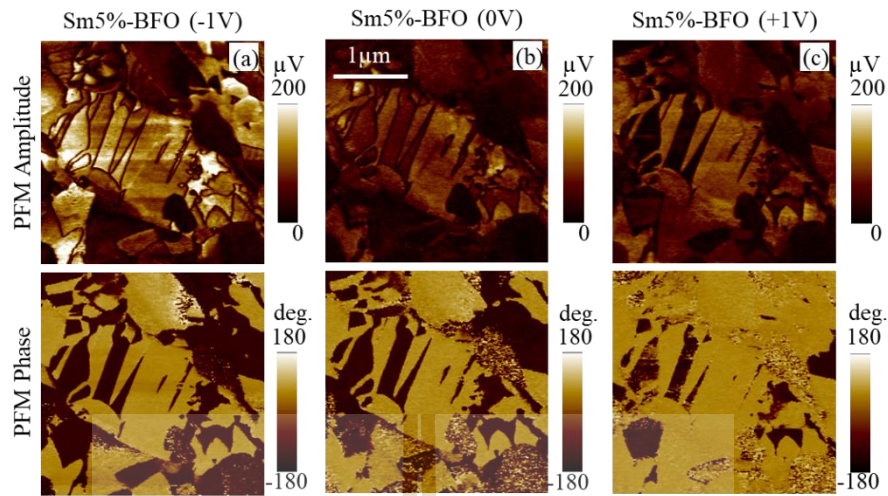


**Figure 3.5** PFM-Amplitude and PFM-Phase of Sm 5% BFO. Image acquired at DC bias = 0 -1 and +1 V ,which show piezoresponse and ferroelectric domain reversion due to external electrical field.

### 3.6 Conductive Atomic Force Microscopy

To study conductivity of the ferroelectric domain, conductive atomic force microscopy (C-AFM) is used. The C-AFM technique is able to perform on the same region as PFM. Voltage bias on tip or sample drive the charge carrier to flow between tip and sample holder. C-AFM can measure current as a function of tip or sample bias and collect the Current-Bias voltage or I-V characteristic to demonstrate diode behavior of BFO.

### 3.7 Images Analysis and Statistical Methods

Image analysis of PFM and C-AFM images are using XEI software, which is Park-AFM software to collect statistical and average value. In this work, we use biological sample collection statistical method (Cumming et al., 2007) to adapt for PFM

and C-AFM to get average  $d_{33}$  and conductivity. We assume the average data is a representative of sample surface. For example, we scan 10 images ( $n = 10$ ) and each image have Root Mean Square (RMS) average value  $V_{rms,1}, V_{rms,2}, V_{rms,3} \dots V_{rms,10}$ , then we calculate a started error (SE) and used as a confident interval. The condition we using to consider stop adding scanning image ( $n$ ) is when new scanning image have average value in the confident interval ( $\pm SE$ ).



# CHAPTER IV

## RESULTS AND DISCUSSION

### 4.1 Barium Titanate Study

Representative topographic atomic force microscopy images obtained from BTO ceramics containing various amounts of AuNPs additive are given in Figure 4.1. In general, the bright and dark contrast in these micrographs represent topological variations of the sample's surface, in analogous to the typical scanning electron microscopy (SEM) image where dark areas represent depressions of the surfaces and brighter areas are relatively higher (Haugstad, 2012). Round-shaped and micron-sized grains, and grain boundary regions are clearly seen in the topographic images of all investigated samples (Fuentes et al., 2010; Silva et al., 2016). Clearly, the topographic image of unmodified (*i.e.* 0.0% AuNPs) BTO ceramics (Figure 4.1(a)) presents several grains with the grain boundaries distinguished by a sharp change in contrast, in agreement with those observed by Buscaglia et al. (Buscaglia et al., 2004). Interestingly, it is likely that individual micron-sized grains of AuNPs-modified samples (Figure 4.1 (b-d)) exhibited the dispersion of nano-sized particles which could be the AuNPs additive. This finding is also similar to those observed by Shen et al. (Shen et al., 2012).

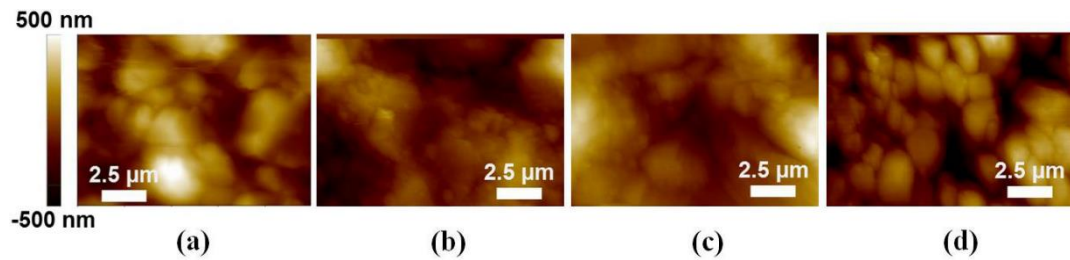


**Figure 4.1** Topographic images of BT ceramics with (a) 0.0%, (b) 2.0%, (c) 4.0% and (d) 8.0% of AuNPs sintered at 1250°C for 2 h.

Moreover, the AuNPs-modified BT samples possessed the uniform microstructure with relatively smaller grain size when compared with the unmodified BT sample, coherent with previous research regarding their corresponding microstructures obtained by SEM technique (Nonkumwong et al., 2015). The estimated grain sizes obviously measured from the 8.0% AuNPs-modified BT samples (Figure 4.1(d)) are in the range of  $\sim 0.6 - 3.1 \mu\text{m}$  while larger grain sizes of unmodified BT ceramics are  $\sim 1.0 - 4.0 \mu\text{m}$ . This observation strongly supported our previous discussion which was mentioned that tailoring of BT ceramics with AuNPs additive could inhibit the ceramic grain-growth, resulting in an increase of dielectric constant (*i.e.* in this case, the magnitude of the dielectric constant strongly depends on the ease of polarization or the dipole switching (Rai et al., 2013)) of the ceramics (Nonkumwong et al., 2015). To further investigate the polarization mechanism related to ferroelectric/piezoelectric properties of the BT ceramics containing various amounts of AuNPs content, PFM technique was conducted for mapping the ferroelectric domains and studying the local polarization switching in which variations in the orientation of the polarization can be distinguished through changes in the phase of the piezoelectric deformation of the sample subjected to the action of an oscillating electric field.

To complete a piezoelectric image, both amplitude and phase parameters have to be carefully monitored as shown in Figure 4.2. For PFM image recording, the conducting tip is scanned in contact mode with upper surface of samples while different  $V_{DC}$  is applied between the tip and Ag electrode at lower surface. As the domains in one grain attempt to switch, they are constrained by the differently oriented neighboring grains. The PFM phase features indicate the changing or inform the information of domain orientation where  $0^\circ$  means in-phase (IP) piezoresponse to the driving voltage, results in an expansion of the domain, while  $180^\circ$  means out-of-phase (OOP) response, results in a contraction of the domain. The PFM phase images for all samples, except 8 % AuNPs-modified BT, indicate that applying positive  $V_{DC}$  (up to 5 V) causes significant  $180^\circ$  phase changes, *i.e.* create more OOP domains, more than applying negative  $V_{DC}$  (Figure 4.2, lower panels). It means that before applying voltage, most of domains point upward to the scanned surfaces (Pramanick et al., 2012). Additionally, when the positive  $V_{DC}$  was applied to unmodified BT samples, the  $90^\circ$  domains seem to be observed. Both  $180^\circ$  and  $90^\circ$  polarization switching of ferroelectric walls can be ascribed to the minimization of the electrostatic energy and the elastic energy, respectively (Cheng et al., 2006). However, the most obvious phase shift ( $180^\circ$  domains) can be observed from applying positive 2.5 V to 4.0% AuNPs-modified BT ceramics. This information indicates that the amount of AuNPs affected on the orientation polarization, *i.e.* the higher amount of AuNPs additive, the more polarization reversal obviousness when the opposite  $V_{DC}$  was applied, revealing superior piezoelectric characteristics. As a consequence, higher dielectric constant values (because of the easier domain switching resulting in higher polarization) could be obtained from the AuNPs-modified BT ceramics than that obtained from unmodified

BT sample, as evidence in previous work (Nonkumwong et al., 2015). Nevertheless, applying unsuitable  $V_{DC}$  for each condition such as applying positive 5 V to 4.0 % AuNPs-modified BT does not provide more phase shift but the opposite result was found. In this case, it might be explained by too much energy from too much applied voltage can cause the creation of newly reverse domains. As a result, their effective piezoelectric coefficients ( $d_{33}$ ) will cancel each other as the integrated effect of two cylindrical head-to-head (tail-to-tail) domains in agreement with Kholkin et al. (Kholkin et al., 2004). In the same way, the reason for no observed phase change by applying positive  $V_{DC}$  only up to 5 V to 8.0% AuNPs-modified BT sample as mentioned above might be due mainly to insufficient energy to create the stable domains of opposite polarity (Kholkin et al., 2004). These observations pointed out that the orientation polarization of the samples might be tailored by applying the negative or positive  $V_{DC}$  dependent on their chemical compositions. By the way, since the different shade is referred to the direction of the polarization projection onto the samples, it can be inferred that all investigated samples have average non-zero piezoresponse in this poled state ( $\pm 5$  V). However, judging from only the phase image cannot provide the exact characteristics such as those found in 8.0% AuNPs-modified BT case where it looked like that no domains exist in the scanning area. Therefore, it is also important to measure the PFM amplitude.

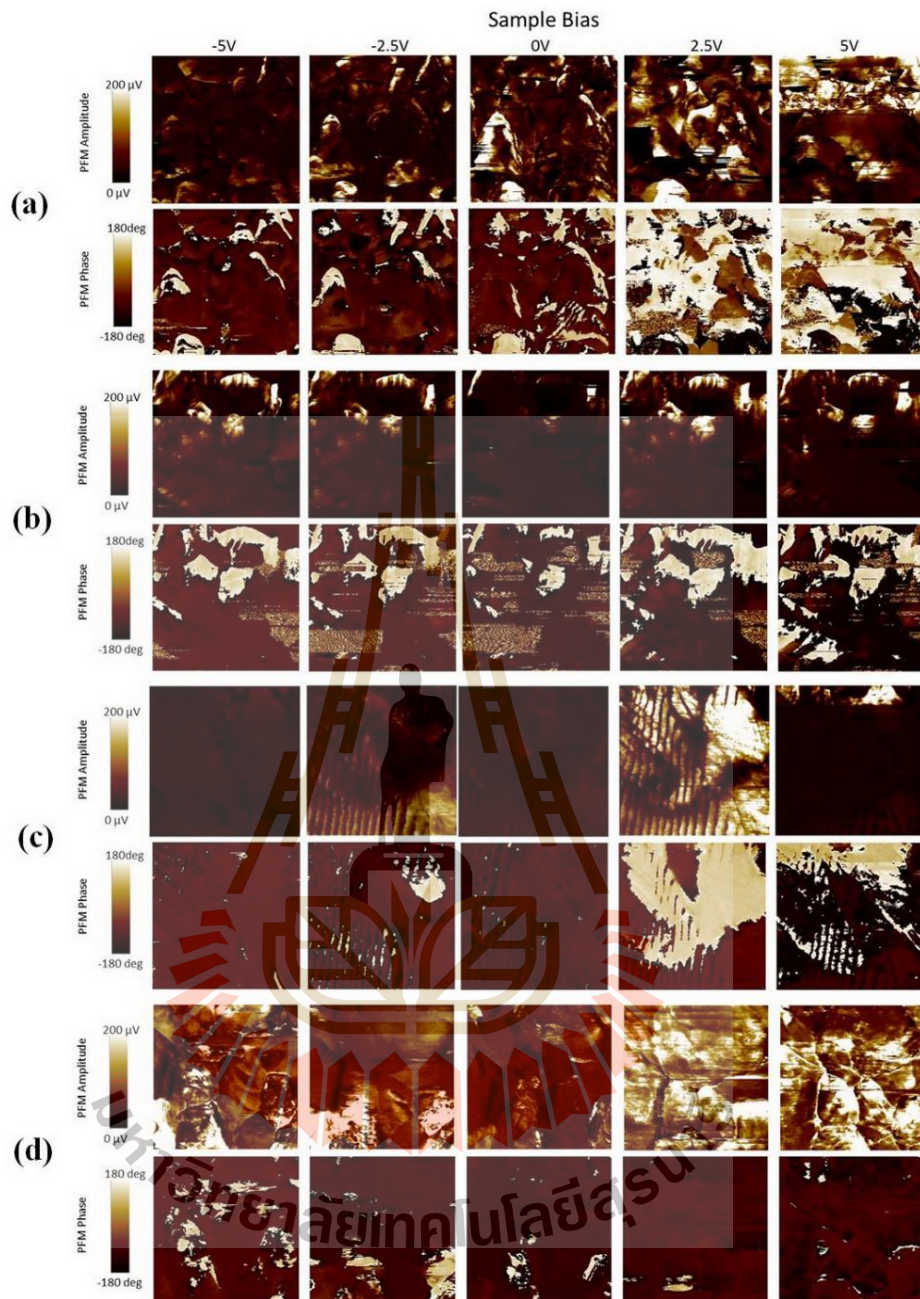


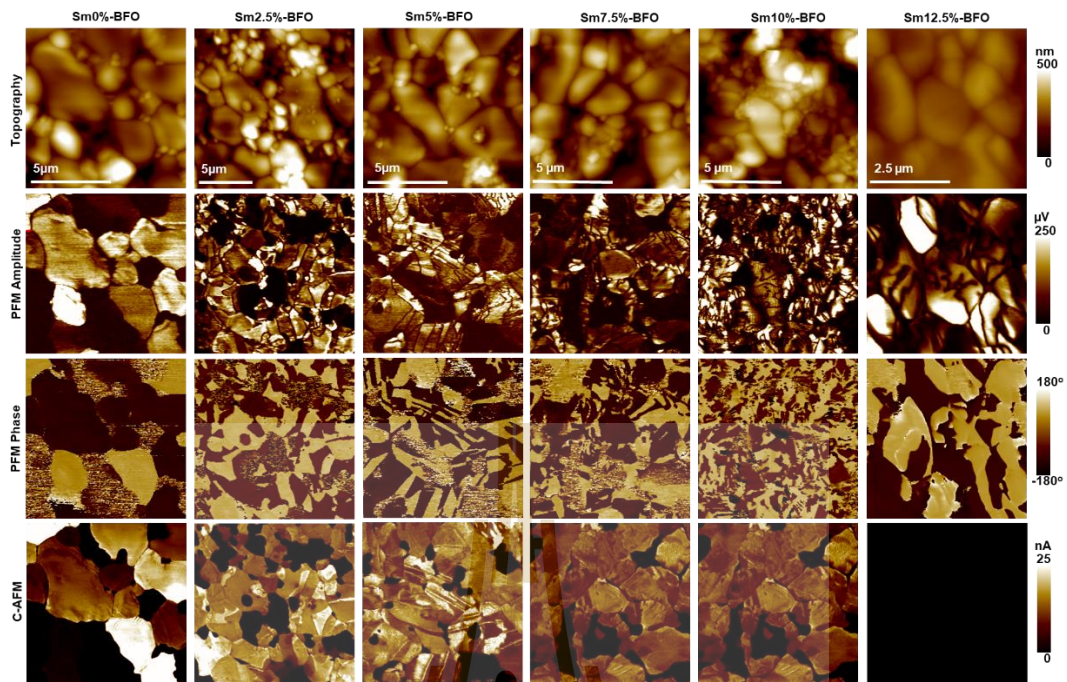
**Figure 4.2** Amplitude (upper panel) and phase contrast (lower panel) PFM images of BT ceramics with (a) 0.0%, (b) 2.0%, (c) 4.0% and (d) 8.0% of AuNPs sintered at 1250°C for 2h.

In this connection, the amplitude piezoresponse images of these samples are also given in Figure 4.2 (upper panels). The different shade in images exhibited different piezoresponse (weak; the darker area and strong; the brighter area) or degree of effective  $d_{33}$  coefficient. By applying positive, all samples exhibit apparently strong piezoresponse more than applying negative  $V_{DC}$ . The strong piezoresponse areas (*i.e.* the brighter area) in 4.0% and 8.0% AuNPs-modified BT ceramics are much larger than that of unmodified and 2.0% AuNPs-modified BT cases. These variations could certainly support the differences in their dielectric properties, as mentioned earlier. This finding especially for 4.0% AuNPs-modified BT sample which show the most obvious phase change as described above could be comparable to Zhao et al. research (Zhao et al., 2015). In this case, they applied a negative bias to Pb-based perovskite ferroelectric system of lead magnesium niobate-lead titanate (PMN-PT) ceramics, with various ratios of PMN/PT, from -10 to -70 V to create a reversed polarity domain and found that the fluctuation of PT content affected on the domain configurations and domain dynamic response. They reported that the reversed polarization of macrodomain area in PMN-35%PT and PMN-25%PT exhibited a relatively higher response behavior and better polarization retention performance than that of microdomain in PMN-10%PT and PMN-20%PT. Again, it was noticeable that applying positive 5 V to 4% AuNPs-modified BT ceramics causes the decreasing of effective  $d_{33}$  coefficient compared with applying only +2.5 V. This finding supports the previous explanation related to the cancellation of the oppositely poled grains exist after applying more than +2.5 V. In contrary to 8.0% AuNPs-modified BT case, although there were not phase changes found in the previous discussion, this sample showed the highest amplitude among others. These results emphasize that it is possible to control the piezoresponse of the

AuNPs-modified BT ceramics by selection the proper applied  $V_{DC}$  for each AuNPs content. Moreover, it is likely that homogeneous polarization state of the ceramics could be induced by applying high bias and/or increasing AuNPs content. However, to obtain a better understanding on ferroelectric domain evolutions and local polarization switching, further research on applying higher voltage as found in Zhao et al. (Zhao et al., 2015) is therefore attractive. Additionally, Kim et al. (Kim and Huber, 2015) work which study the ferroelastic domain evolution under compressive loading in polycrystalline lead zirconate titanate (PZT) ceramics by using PFM also provided the interesting point to apply this method for our AuNPs-modified BT samples because their results confirmed that applying different compressive loading revealed the involved multiple domain switching processes. With these understandings, the fundamental necessity both for the development of novel materials and an improvement of their potential device performances as aimed could be surely achieved.

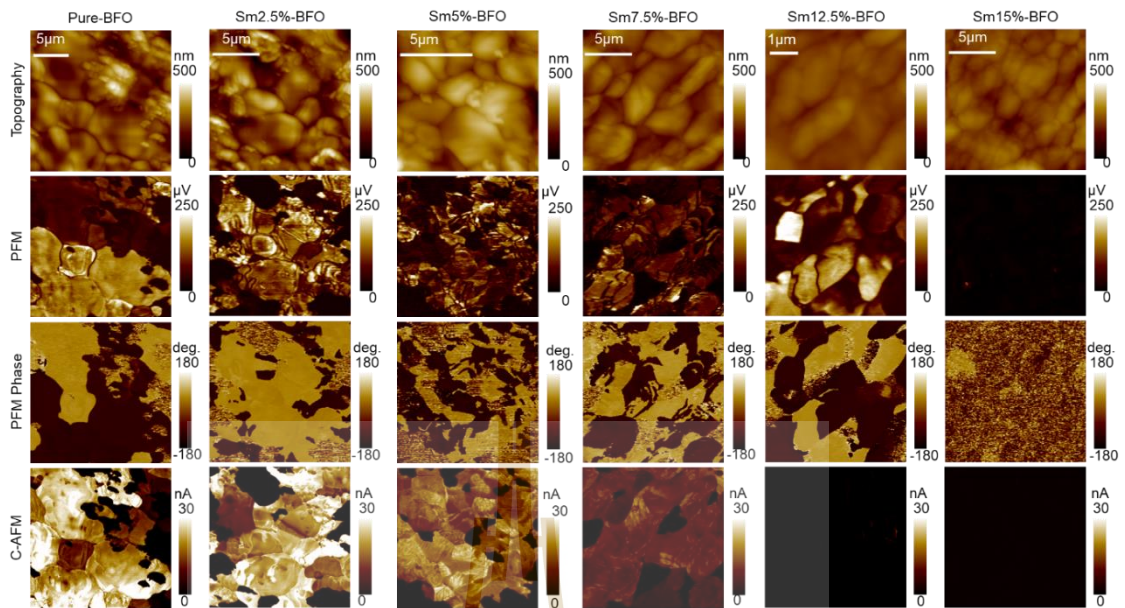
## 4.2 PFM and C-AFM Studies of Sm-substituted BFO

Figure 4.3 shows topography, PFM amplitude, PFM phase and C-AFM images of  $\text{Bi}_{1-x}\text{Sm}_x\text{FeO}_3$  ( $x = 0, 0.025, 0.05, 0.075, 0.100$  and  $0.125$ ) samples. The topography show roughness of sample surface at difference doping. Grain size on surface have decrease as a function of Sm doping. The amount of small grains decreased corresponding to the impurity phase characterized by XRD.



**Figure 4.3** PFM results of BFO sample from Sm 0 -12.5%.

To discuss in to detail, Figure 4.5 shows AFM, PFM and C-AFM images of  $\text{Bi}_{1-x}\text{Sm}_x\text{FeO}_3$  ( $x = 0, 0.050, 0.075, \text{ and } 0.125$ ) samples. From the AFM images, the BFO ceramics are made of grains with difference sizes. A plot of average grain size for different samples is summarized in a Figure 2.1. In the Sm 0% sample, we observed two types of grains: large grains with diameter about  $8 \mu\text{m}$  and small particles with diameter about  $1 \mu\text{m}$  clustered between the edges of the big grains. Since there are less amount of large grains per area, they appear as outliers in the plot. The grain size decreases as the doping level increases, which is attributed to the reduced in the volatile Bi ions (Makhdoom et al., 2012; Yotburut et al., 2017). For Sm 5% - 7.5% samples, the grain size is about  $3 \mu\text{m}$  and the small particles are still observed. At 12.5% Sm sample, the grain size is rather uniform,  $\sim 1 \mu\text{m}$ .



**Figure 4.4:** Topography, PFM Amplitude, PFM Phase, and C-AFM images of  $\text{Bi}_{1-x}\text{Sm}_x\text{FeO}_3$  ( $x = 0 - 0.150$ ) samples at various locations. The scale bars are  $5 \mu\text{m}$  for the Sm 0% - 10%, 15% images,  $1 \mu\text{m}$  for the Sm 12.5% images.

When comparing the PFM amplitude, PFM phase and C-AFM images of the Sm 0% sample (Figure 4.5(e), (i), and (m)), we found no correlation between the polarization direction and conductivity. For example, the grains marked by the white dash and white solid lines are both down domains but have different current signals. The domains in the grains marked by the red dash and red solid lines are both up domains, but only that marked by the red solid line has current signal

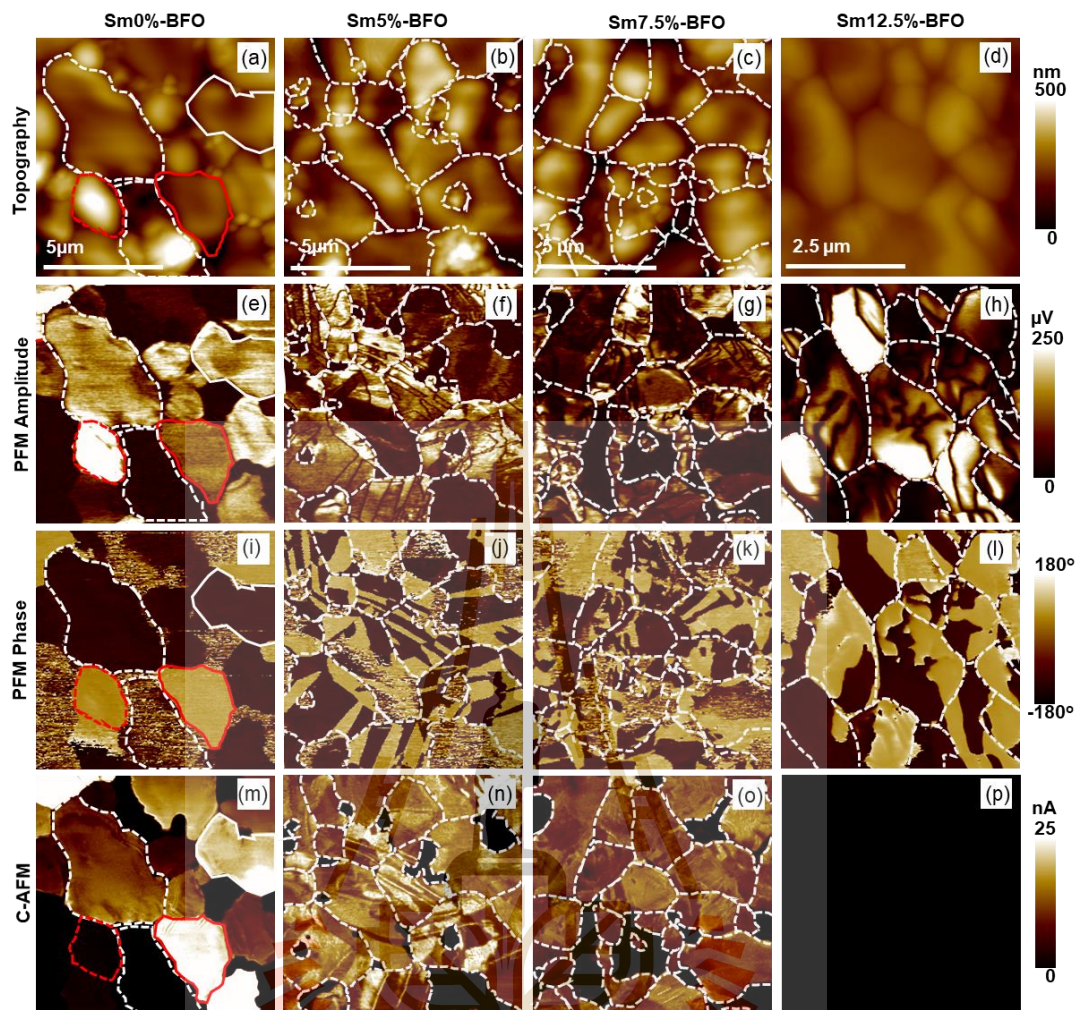


**Figure 4.5** (a) - (d) Topography, (e)-(h) PFM Amplitude, (i) - (l) PFM Phase, and (m) - (p) C-AFM images of  $\text{Bi}_{1-x}\text{Sm}_x\text{FeO}_3$  ( $x = 0, 0.050, 0.075,$  and  $0.125$ ) samples. The arrow points to the  $1 \mu\text{m}$  particles located between the big grains. The white-dotted line indicates regions with zero response in both PFM and C-AFM channels. Red and white lines outline grains from the topography images with different PFM and C-AFM responses (see main text for details). The scale bar are  $5 \mu\text{m}$  and  $2.5 \mu\text{m}$  for the Sm 0% - 7.5% and Sm 12.5% images, accordingly.

Moreover, closer inspection reveals some correlation between the polarization direction and conductivity. Domains with polarization down (dark color in the PFM

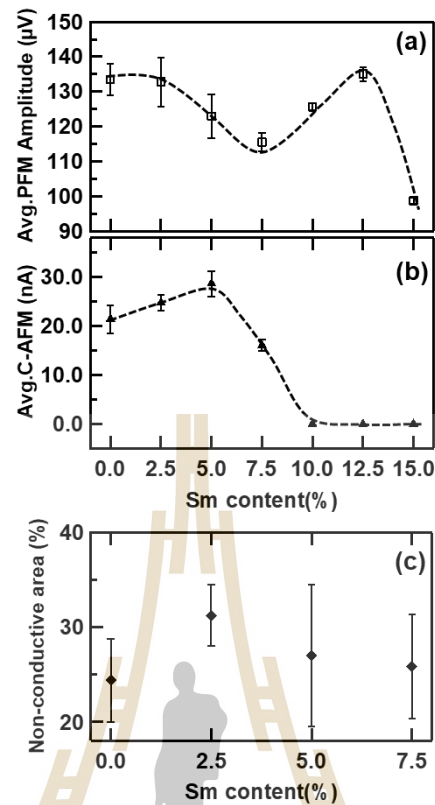


**Figure 4.6** (a) – (b) average PFM response and average C-AFM signal as a function of Sm content for  $\text{Bi}_{1-x}\text{Sm}_x\text{FeO}_3$  ( $x = 0 - 0.150$ ). For the average C-AFM signal, the regions excluding the non-conducting regions were used. The lines are guide to the eyes. (c) Areal fraction of the non-conducting region for  $x = 0 - 0.075$ .

phase image, Figure 4.5(j)) are slightly more conductive than the domains with polarization up (light color in the PFM phase). Such polarization-modulated conductivity is similar to what has been observed in BFO films (Chen et al., 2007; Kim et al., 2012; Lee et al., 2011; Wang et al., 2011). Here, the effect is weaker since the electric field is smaller in our thick ceramic samples. However, exception are found, for example, the grain that has both up and down domains, but C-AFM signal are rather similar. We speculate that the conductivities of these domains are also influenced by local surface charges or the domain polarization change to the same direction under the

bias. Similar behavior is seen in the Sm 7.5% sample, though the average C-AFM signal is lower. Attempting to extract the correlation coefficient between the PFM images and C-AFM images give no significant results since the up and down domains only have small conductivity difference as showed by low conductivity correlation in Figure 4.7.

Figure 4.5(a) – (b) summarize the average PFM and C-AFM responses as a function of Sm-content. For, the average PFM response, we use signals from the entire images. For the average C-AFM response, we excluded the regions with current signal lower than the noise level 1 nA. The error bars were calculate from images at different locations. The average PFM response drops a little at 7.5% Sm doping, and raises again at 12.5% and diminishes at 15% Sm doping. Average C-AFM responses are similar for the Sm 0 – 5% sample. The decreased grain size does not interrupt conductive paths and lower the conductivity as oppose to observation from other study (Lubomirsky et al., 2002). A drop in the PFM response at 7.5% is accompanied by lower average C-AFM response (Figure 4.5(b)). The current signal disappears at higher doping level at Sm-substitution higher than 10%. At Sm 12.5% substitution, the sample has large piezoresponse, but low leakage, a desirable property for applications.

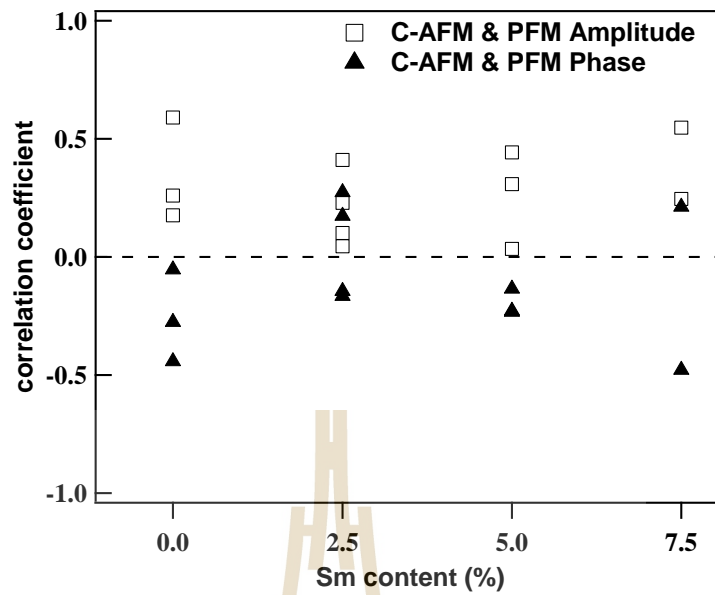


**Figure 4.7** Correlation of C-AFM, PFM phase, and PFM amplitude.

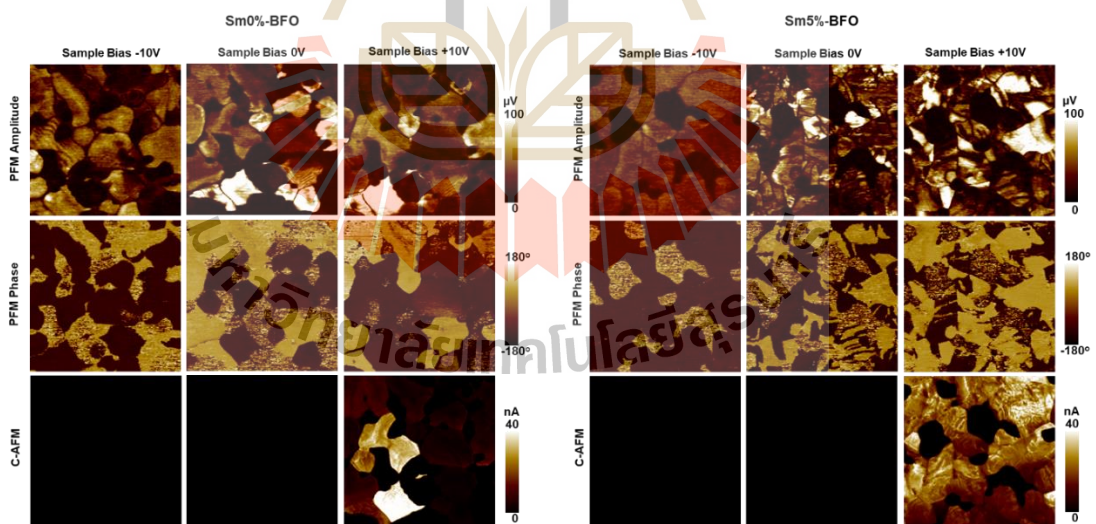
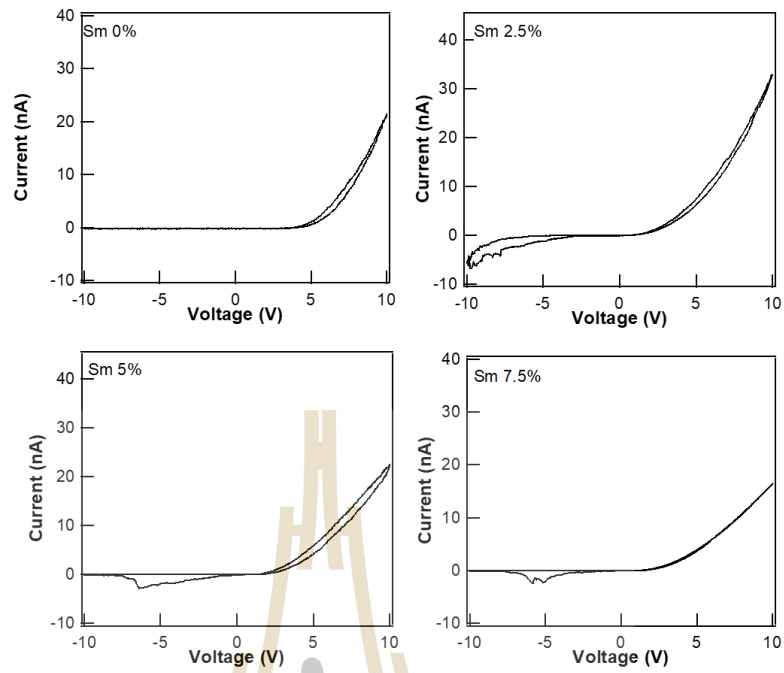


**Figure 4.8** PFM and C-AFM images of Sm 0% and 5% samples taken at sample bias = 0, +10 V and -10 V.

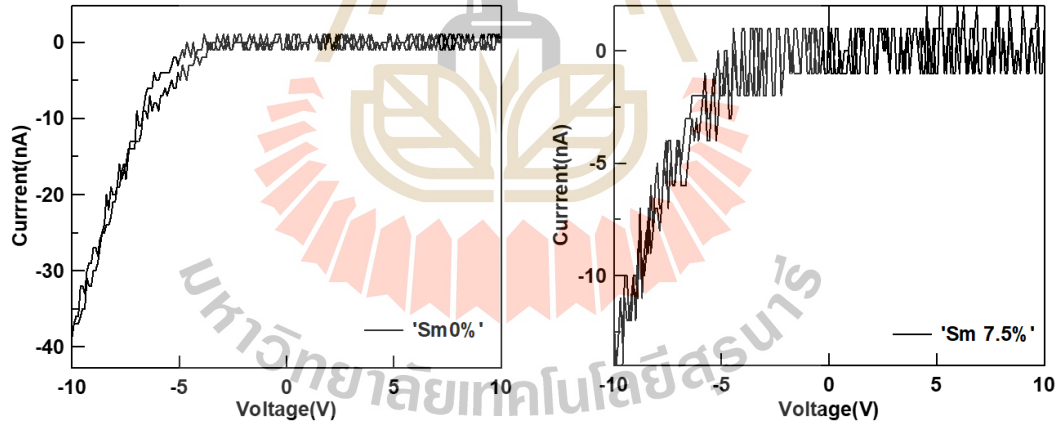
### 4.3 Transport Properties of Sm-substituted BFO

Figure 4.11(a) shows typical  $I$ - $V$  curves plotted on semi-logarithmic scales taken at conductive domains in the Sm 0 – 7.5% Sm samples. All  $I$ - $V$  curves show rectifying behavior with the forward current when applying positive bias to  $V_{sample}$  ( $I$ - $V$  curves when applying tip bias see Figure 4.10). Small hysteresis was observed (see Figure 4.8) and will be the subject of future study. The  $I$ - $V$  curves indicate a p-type carriers at the tip-sample interface (Choi et al., 2009; Lee et al., 2011; Miranda et al., 2014). This different from a hot point probe test, which shows a bulk n-type carrier for all samples. Different carrier type at the metal-sample interface from the bulk was observed in other ferroelectric materials (Pintilie and Alexe, 2005). For this sample, it can be explained an accumulation of the Bi and Fe vacancies (Pintilie and Alexe, 2005; Yang et al., 2009) at the interface.

The  $I$ - $V$  characteristic of Sm-substitute BFO are divided into two regimes. At  $V_{sample} < 3$  -7 V, the current increase exponentially suggesting a Schottky-like barrier at the tip-sample interface (Miranda et al., 2014; Wu et al., 2010). Fitting the  $I$ - $V$  curves to the Schottky diode equation  $I = I_s (\exp(eV/\beta k_B T) - 1)$ , where  $V$  is the voltage at the junction,  $I_s$  is saturation current,  $e$  is electron charge,  $\beta$  is ideality factor,  $k_B$  is Boltzmann constant, and  $T$  is the temperature. Since, our  $I$ - $V$  curves shows current above the noise level at an offset voltage  $V_o$ , it is appropriate to use a correct  $V_{sample}$  by  $V_o$ . Figure 4.11 (b) plots  $V_o$  as a function of Sm-content.  $V_o = 4.5$  V for the Sm 0% sample, and  $V_o = 1$  – 2.5 V for the Sm 2.5% – 7.5% samples. The higher offset  $V_o$  for the Sm 0% sample suggests larger screening effect in the bulk, likely from higher amount of oxygen vacancies.



**Figure 4.9** Hysteresis loop in I-V characteristic.



**Figure 4.10** Tip bias I-V characterization.

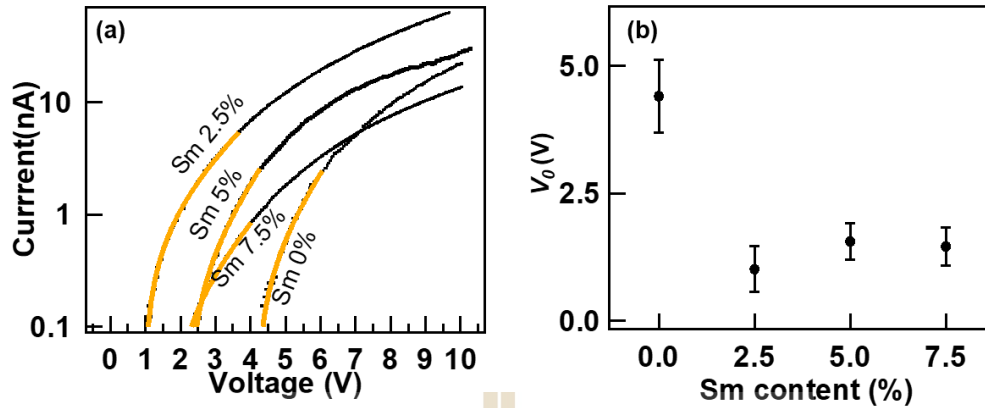


**Figure 4.11** (a) I-V curves of ferroelectric domains  $\text{Bi}_{1-x}\text{Sm}_x\text{FeO}_3$  ( $x = 0 - 0.075$ ). The solid lines are exponential fits. (b) Offset voltages ( $V_o$ ) extracted from the I-V curves as a function of Sm content.

We obtained  $\beta \sim 45$  for all samples. The ideality factor much larger than 1 were found in previous studies (Choi et al., 2009; Wu et al., 2010) and were attributed to two factors: highly doped sample or defective p-n junctions (Scott, 2009). Since the ideality factor remains the same across different doping level, we believe that the large ideality factor are likely due to defects. Therefore, the voltage at the junction is given by  $V = V_{\text{sample}} - V_o$ . Furthermore, at  $V > 1$  V, the I-V curves deviate from the diode equation and can be described by space-charge limited conduction (SCLC). Figure 4.12 shows a double log plots of the I-V curves, which give a straight light indicating the and  $I \propto V^n$ . The slope of the double log plot is the power,  $n$ . We obtained  $n \sim 2.6 - 3.1$ . The  $n > 2$  is referred as a trap-controlled SCLC (Lampert and Schilling, 1970).

The p-type rectifying behavior also explained the different conductivity for the up and down polarization seen in the Sm 5% sample (Figure 3.5). Figure 4.6(c) shows a band diagram at the tip-sample interface under a low forward bias,  $3 > V_{\text{sample}} > 0$ . Positive charge accumulation at the surface bends the band downward at the junction

with some barrier potential, and the applied voltage lower the barrier causing the current to flow. For the domain with polarization up, there is more accumulation of positive charge, which further lower the barrier potential. The barrier is higher in the domain with polarization down. Applying the negative sample bias  $V_{sample} < 0$ , increases the barrier height, thus no current flow. We emphasize that the voltage at the junction is much lower due to the screening effect of oxygen vacancies. This also explain why no polarization-modulation conductivity was observed in the Sm 0% BFO sample.

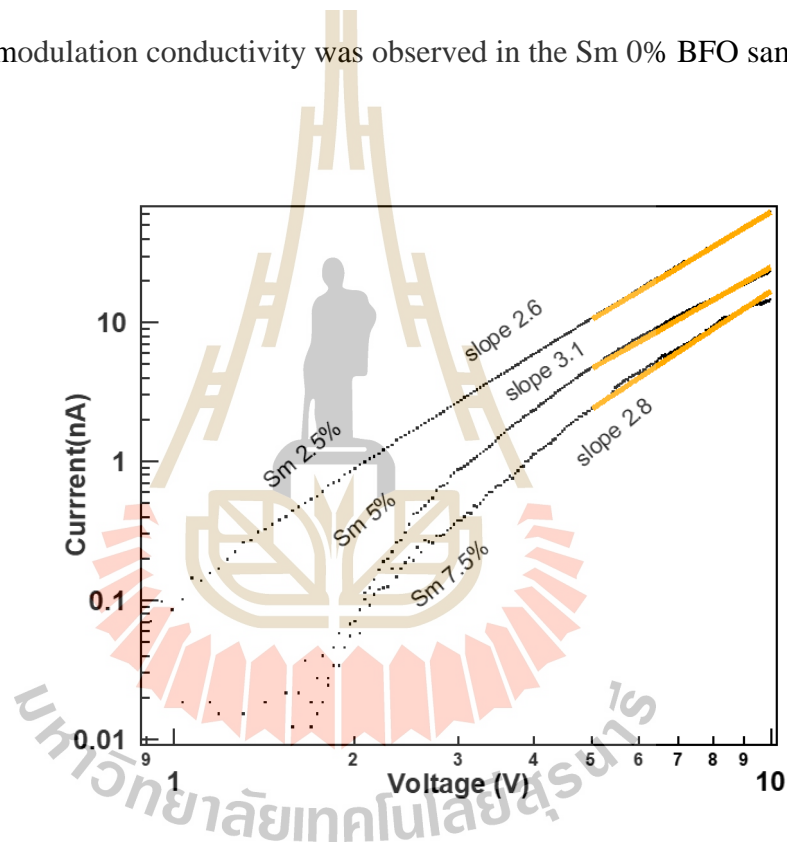


**Figure 4.12** Double log plot of the curves from  $x = 0.025 - 0.075$  sample, which show linear dependence at high voltage.

# CHAPTER V

## CONCLUSIONS

### 5.1 Sm-BFO Study

In summary, we performed PFM and C-AFM study of Sm- substituted BFO ceramics, doping level 0 - 15%, growth by co-precipitation method. XRD spectrums indicate structural transition from rhombohedral to orthorombic at Sm 15% doping. Sm-substitution has two consequences to BFO. First, it decreases the  $\text{Bi}_2\text{Fe}_4\text{O}_9$  phase at in the  $\geq$  Sm 7.5% samples as seen in the XRD spectrums. The second consequence is seen from the transport behaviors. For Sm 10% – 12.5% samples, the leakage greatly decrease, while the piezoresponse remain high due to decreased chemical defects. In the Sm 0% – 7.5% samples, the ferroelectric domains are conductive with defect-dominate transport properties. Weak polarization-modulation rectifying behavior is seen in the Sm 2.5% and 5% samples. Transport behaviors of the domains shows interface-dominate Schottky conduction at low voltage and SCLC at higher voltage. The tip-sample interface exhibit p-type rectifying behavior differ from the n-type bulk suggesting accumulation of the positively charge defects at the interface. The Schottky conduction is offset by an offset voltage with the largest value in the Sm 0% sample, indicating screening effect from the bulk.

## 5.2 AuNPs-BT Study

For barium titanate, Piezoresponse force microscopy was adopted to study the complex domain evolution in polycrystalline BT-based ceramics containing various amounts of AuNPs additives. Complex microstructures that are agglomerations of a very large number of variously oriented grains were evidenced. Additive content dependence was noticeable in AuNPs-modified BTO ceramics where higher amplitude can be observed from applying positive  $V_{DC}$  to 0.4% AuNPs-modified BTO ceramics, compared to other samples, revealing more polarization reversal obviousness, i.e. Superior piezoelectric characteristics. The amplitude piezoresponse images indicate that most samples exhibit stronger piezoresponse by applying positive  $V_{DC}$  than that by negative  $V_{DC}$ . Interestingly, the strong piezoresponse areas of AuNPs-modified BTO ceramics are larger than that of unmodified BT case indicating the possibility of control the polarization switching of the AuNPs-modified BT ceramics by a selection of the proper applied  $V_{DC}$ .

For BTO sample, AuNPs-modified BTO ceramics have polarization reversal when we bias minus more than plus voltage. This behavior indicates the potentials in a memory application, however the bulk or ceramics form is not practical in nanoscale memory. We expected to study thin films of BTO in the future.

## 5.3 Future Works

Future study, test and experimental have been left for the future due to the lack of time and restriction of instruments. Future works concerns deeper analysis of particular mechanisms, more data acquisitions, and simply curiosity.

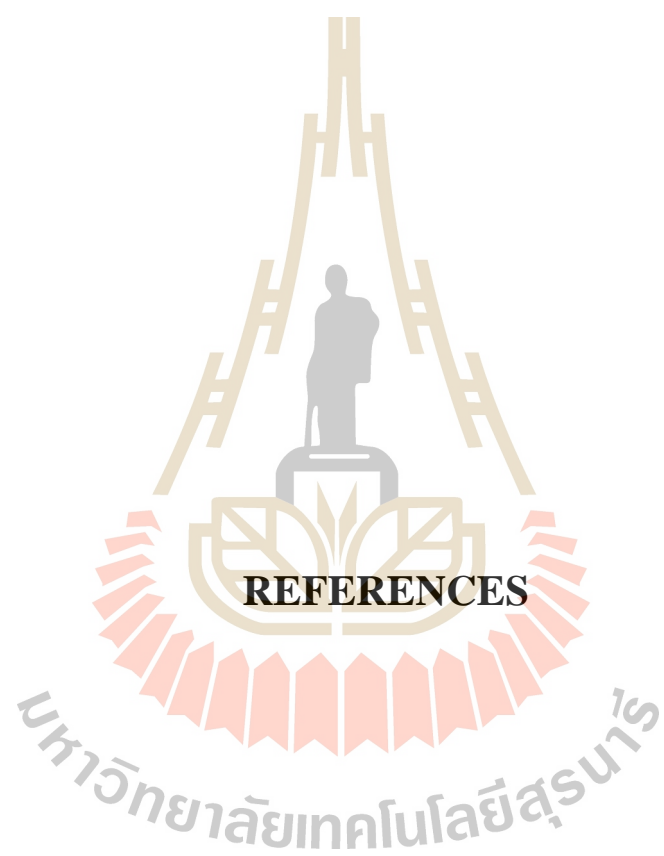
There are some idea that rushed into mind and I would like to try during the work. This thesis are mainly focus on ceramics and in plan ferroelectric domains, but the better way to study is considering both in plan (IP) and out of plan (OOP) ferroelectric domains. The following idea could be tested:

Firstly, despite an output of scanning probe microscopy have one output channel, but we could consider to use two output SPM model to acquire both IP and OOP domain. We could interpret complete polarization direction and predict the domain wall properties.

Secondly, obviously we study ceramics of polycrystalline bismuth ferrite (BFO) and barium titanate (BTO), however we could study thin film BTO and BTO to compare the phenomena of stress and thinness affect for polarization magnitude.

Thirdly, more advanced mode of SPM, Microwave Impedance Microscopy (MIM), could address the dielectric constant and conductivity simultaneously. With MIM we can investigate the dielectric effect in electrical loss and polarization simultaneously.

In the future, we could perform the investigation in dielectric constant and local hysteresis loop analysis, we could achieved a reduction of a secondary phase and defect in polycrystalline and thin film BFO. We attempt to research more and push the BFO and BTO into the applications.



## REFERENCES

- Alikin, D., Turygin, A., Walker, J., Rojac, T., Shvartsman, V. V., Shur, V. Y. and Kholkin, A. L. (2015). Quantitative phase separation in multiferroic Bi<sub>0.88</sub>Sm<sub>0.12</sub>FeO<sub>3</sub> ceramics via piezoresponse force microscopy. **Journal of Applied Physics**. 118(7): 072004.
- Buscaglia, M. T., Buscaglia, V., Viviani, M., Petzelt, J., Savinov, M., Mitoseriu, L., Testino, A., Nanni, P., Harnagea, C. and Zhao, Z. (2004). Ferroelectric properties of dense nanocrystalline BaTiO<sub>3</sub> ceramics. **Nanotechnology**. 15(9): 1113.
- Catalan, G. and Scott, J. F. (2009). Physics and Applications of Bismuth Ferrite. **Advanced Materials**. 21(24): 2463-2485.
- Cazayous, M., Malka, D., Lebeugle, D. and Colson, D. (2007). Electric field effect on Bi Fe O<sub>3</sub> single crystal investigated by Raman spectroscopy. **Applied Physics Letters**. 91(7): 071910.
- Chen, Y., Katz, M., Pan, X., Das, R., Kim, D., Baek, S. and Eom, C. (2007). Ferroelectric domain structures of epitaxial (001) Bi Fe O<sub>3</sub> thin films. **Applied Physics Letters**. 90(7): 072907.
- Cheng, C.-J., Kan, D., Anbusathaiah, V., Takeuchi, I. and Nagarajan, V. (2010). Microstructure-electromechanical property correlations in rare-earth-substituted BiFeO<sub>3</sub> epitaxial thin films at morphotropic phase boundaries. **Applied Physics Letters**. 97(21): 212905.

- Cheng, S. Y., Ho, N. J. and Lu, H. Y. (2006). Transformation- Induced Twinning: The 90° and 180° Ferroelectric Domains in Tetragonal Barium Titanate. **Journal of the American Ceramic Society**. 89(7): 2177-2187.
- Choi, T., Lee, S., Choi, Y., Kiryukhin, V. and Cheong, S.-W. (2009). Switchable ferroelectric diode and photovoltaic effect in BiFeO<sub>3</sub>. **Science**. 324(5923): 63-66.
- Coondoo, I., Panwar, N., Bdikin, I., Puli, V., Katiyar, R. and Kholkin, A. (2012). Structural, morphological and piezoresponse studies of Pr and Sc co-substituted BiFeO<sub>3</sub> ceramics. **Journal of Physics D: Applied Physics**. 45(5): 055302.
- Cumming, G., Fidler, F. and Vaux, D. L. (2007). Error bars in experimental biology. **The Journal of cell biology**. 177(1): 7-11.
- Daraktchiev, M., Catalan, G. and Scott, J. (2008). Landau theory of ferroelectric domain walls in magnetoelectrics. **Ferroelectrics**. 375(1): 122-131.
- Das, R., Sarkar, T. and Mandal, K. (2012). Multiferroic properties of Ba<sup>2+</sup> and Gd<sup>3+</sup> co-doped bismuth ferrite: magnetic, ferroelectric and impedance spectroscopic analysis. **Journal of Physics D: Applied Physics**. 45(45): 455002.
- Dawber, M., Rabe, K. M. and Scott, J. F. (2005). Physics of thin-film ferroelectric oxides. **Reviews of Modern Physics**. 77(4): 1083-1130.
- Devonshire, A. F. (1949). XCVI. Theory of barium titanate. **The London, Edinburgh, and Dublin Philosophical Magazine and Journal of Science**. 40(309): 1040-1063.
- Devonshire, A. F. (1951). CIX. Theory of barium titanate—Part II. **The London, Edinburgh, and Dublin Philosophical Magazine and Journal of Science**. 42(333): 1065-1079.

- Diéguez, O., González-Vázquez, O., Wojdeł, J. C. and Íñiguez, J. (2011). First-principles predictions of low-energy phases of multiferroic BiFeO<sub>3</sub>. **Physical Review B**. 83(9): 094105.
- Directive, E. (2011). Directive 2011/65/EU of the European Parliament and of the Council of 8 June 2011, on the restriction of the use of certain hazardous substances in electrical and electronic equipment (recast). **Official Journal of the European Communities**.
- Directive, R. (2003). Directive 2002/95/EC of the European Parliament and of the Council of 27 January 2003 on the restriction of the use of certain hazardous substances in electrical and electronic equipment. **Official Journal of the European Union**. 13: L37.
- Eerenstein, W., Mathur, N. and Scott, J. F. (2006). Multiferroic and magnetoelectric materials. **Nature**. 442(7104): 759.
- Filippetti, A. and Hill, N. A. (2002). Coexistence of magnetism and ferroelectricity in perovskites. **Physical Review B**. 65(19): 195120.
- Forrester, J., Kisi, E. and Studer, A. (2005). Direct observation of ferroelastic domain switching in polycrystalline BaTiO<sub>3</sub> using in situ neutron diffraction. **Journal of the European Ceramic Society**. 25(4): 447-454.
- Fuentes, S., Zárate, R., Chávez, E., Munoz, P., Ayala, M., Espinoza-González, R. and Leyton, P. (2010). Synthesis and characterization of BaTiO<sub>3</sub> nanoparticles in oxygen atmosphere. **Journal of Alloys and Compounds**. 505(2): 568-572.
- Fujino, S., Murakami, M., Anbusathaiah, V., Lim, S.-H., Nagarajan, V., Fennie, C. J., Wuttig, M., Salamanca-Riba, L. and Takeuchi, I. (2008). Combinatorial

- discovery of a lead-free morphotropic phase boundary in a thin-film piezoelectric perovskite. **Applied Physics Letters**. 92(20): 202904.
- Goldschmidt, V. M. (1926). Die gesetze der krystallochemie. **Naturwissenschaften**. 14(21): 477-485.
- Gruverman, A. and Kalinin, S. V. (2006). Piezoresponse force microscopy and recent advances in nanoscale studies of ferroelectrics. **Journal of Materials Science**. 41(1): 107-116.
- Güthner, P. and Dransfeld, K. (1992). Local poling of ferroelectric polymers by scanning force microscopy. **Applied Physics Letters**. 61(9): 1137-1139.
- Haugstad, G. (2012). Atomic force microscopy: understanding basic modes and advanced applications. Trans. Ed. Eds. ed., John Wiley & Sons.
- Hu, Z., Li, M., Yu, B., Pei, L., Liu, J., Wang, J. and Zhao, X. (2009). Enhanced multiferroic properties of BiFeO<sub>3</sub> thin films by Nd and high-valence Mo co-doping. **Journal of Physics D: Applied Physics**. 42(18): 185010.
- Jaffe, B. (2012). Piezoelectric ceramics. Trans. Ed. Eds. ed., **Elsevier**.
- Jaffe, H. (1950). Titanate Ceramics for Electromechanical Purposes. **Industrial & Engineering Chemistry**. 42(2): 264-268.
- Jun, Y.-K., Moon, W.-T., Chang, C.-M., Kim, H.-S., Ryu, H. S., Kim, J. W., Kim, K. H. and Hong, S.-H. (2005). Effects of Nb-doping on electric and magnetic properties in multi-ferroic BiFeO<sub>3</sub> ceramics. **Solid State Communications**. 135(1-2): 133-137.
- Jungk, T., Hoffmann, Á., Fiebig, M. and Soergel, E. (2010). Electrostatic topology of ferroelectric domains in YMnO<sub>3</sub>. **Applied Physics Letters**. 97(1): 012904.

- Kalinin, S. V., Rar, A. and Jesse, S. (2006). A decade of piezoresponse force microscopy: progress, challenges, and opportunities. **IEEE transactions on ultrasonics, ferroelectrics, and frequency control**. 53(12).
- Kan, D., Cheng, C.-J., Nagarajan, V. and Takeuchi, I. (2011). Composition and temperature-induced structural evolution in La, Sm, and Dy substituted BiFeO<sub>3</sub> epitaxial thin films at morphotropic phase boundaries. **Journal of Applied Physics**. 110(1): 014106.
- Kan, D., Pálová, L., Anbusathaiah, V., Cheng, C. J., Fujino, S., Nagarajan, V., Rabe, K. M. and Takeuchi, I. (2010a). Universal Behavior and Electric-Field-Induced Structural Transition in Rare-Earth-Substituted BiFeO<sub>3</sub>. **Advanced Functional Materials**. 20(7): 1108-1115.
- Kan, D., Pálová, L., Anbusathaiah, V., Cheng, C. J., Fujino, S., Nagarajan, V., Rabe, K. M. and Takeuchi, I. (2010b). Universal behavior and electric- field- induced structural transition in rare- earth- substituted BiFeO<sub>3</sub>. **Advanced Functional Materials**. 20(7): 1108-1115.
- Kao, K. C. (2004). Dielectric phenomena in solids. Trans. Ed. Eds. ed., **Elsevier**.
- Kholkin, A. L., Bdikin, I. K., Shvartsman, V. V., Orlova, A., Kiselev, D., Bogomolov, A. A. and Kim, S. H. (2004). Local electromechanical properties of ferroelectric materials for piezoelectric applications. **MRS Proceedings**. 838: O7.6.
- Khomchenko, V., Karpinsky, D., Kholkin, A., Sobolev, N., Kakazei, G., Araujo, J., Troyanchuk, I., Costa, B. and Paixao, J. (2010). Rhombohedral-to-orthorhombic transition and multiferroic properties of Dy-substituted BiFeO<sub>3</sub>. **Journal of Applied Physics**. 108(7): 074109.

- Khomchenko, V. A., Paixão, J. A., Shvartsman, V. V., Borisov, P., Kleemann, W., Karpinsky, D. V. and Kholkin, A. L. (2010). Effect of Sm substitution on ferroelectric and magnetic properties of BiFeO<sub>3</sub>. **Scripta Materialia**. 62(5): 238-241.
- Kim, K. and Huber, J. E. (2015). In situ observation of ferroelastic domain evolution in a near-morphotropic Pb (Zr, Ti) O<sub>3</sub> ceramic by piezoresponse force microscopy. **Journal of the European Ceramic Society**. 35(5): 1459-1468.
- Kim, T. H., Jeon, B. C., Min, T., Yang, S. M., Lee, D., Kim, Y. S., Baek, S. H., Saenrang, W., Eom, C. B. and Song, T. K. (2012). Continuous Control of Charge Transport in Bi- Deficient BiFeO<sub>3</sub> Films Through Local Ferroelectric Switching. **Advanced Functional Materials**. 22(23): 4962-4968.
- Lallart, M. (2011). Ferroelectrics-physical effects. Tech, Croatia.
- Lebeugle, D., Colson, D., Forget, A., Viret, M., Bonville, P., Maruccio, J.-F. and Fusil, S. (2007). Room-temperature coexistence of large electric polarization and magnetic order in Bi Fe O<sub>3</sub> single crystals. **Physical Review B**. 76(2): 024116.
- Lee, D., Baek, S. H., Kim, T. H., Yoon, J. G., Folkman, C. M., Eom, C. B. and Noh, T. W. (2011). Polarity control of carrier injection at ferroelectric/metal interfaces for electrically switchable diode and photovoltaic effects. **Physical Review B**. 84(12): 125305.
- Lobo, R., Moreira, R., Lebeugle, D. and Colson, D. (2007). Infrared phonon dynamics of a multiferroic Bi Fe O<sub>3</sub> single crystal. **Physical Review B**. 76(17): 172105.
- Lubomirsky, I., Fleig, J. and Maier, J. (2002). Modeling of space-charge effects in nanocrystalline ceramics: The influence of geometry. **Journal of Applied Physics**. 92(11): 6819-6827.

- Makhdoom, A., Akhtar, M., Rafiq, M. and Hassan, M. (2012). Investigation of transport behavior in Ba doped BiFeO<sub>3</sub>. **Ceramics International**. 38(5): 3829-3834.
- Miranda, E., Jiménez, D., Tsurumaki-Fukuchi, A., Blasco, J., Yamada, H., Suñé, J. and Sawa, A. (2014). Modeling of hysteretic Schottky diode-like conduction in Pt/BiFeO<sub>3</sub>/SrRuO<sub>3</sub> switches. **Applied Physics Letters**. 105(8): 082904.
- Mishra, R., Pradhan, D. K., Choudhary, R. and Banerjee, A. (2008). Effect of yttrium on improvement of dielectric properties and magnetic switching behavior in BiFeO<sub>3</sub>. *Journal of Physics: Condensed Matter*. 20(4): 045218.
- Mitsui, T. and Furuichi, J. (1953). Domain Structure of Rochelle Salt and K H<sub>2</sub> P O<sub>4</sub>. **Physical Review**. 90(2): 193.
- Moreau, J.-M., Michel, C., Gerson, R. and James, W. J. (1971). Ferroelectric BiFeO<sub>3</sub> X-ray and neutron diffraction study. **Journal of Physics and Chemistry of Solids**. 32(6): 1315-1320.
- Nalwa, K., Garg, A. and Upadhyaya, A. (2008). Effect of samarium doping on the properties of solid-state synthesized multiferroic bismuth ferrite. **Materials Letters**. 62(6-7): 878-881.
- Nonkumwong, J., Ananta, S. and Srisombat, L. (2015). Influence of nanogold additives on phase formation, microstructure and dielectric properties of perovskite BaTiO<sub>3</sub> ceramics. **Applied Physics A**. 119(3): 891-898.
- Nonkumwong, J., Sriboriboon, P., Kundhikanjana, W., Srisombat, L. and Ananta, S. (2018). Ferroelectric domain evolution in gold nanoparticle-modified perovskite barium titanate ceramics by piezoresponse force microscopy. **Integrated Ferroelectrics**. 187(1): 210-218.

- Nonkumwong, J., Srisombat, L. and Ananta, S. (2014). Effect of sintering temperature on phase formation, microstructure and dielectric properties of nanogold modified barium titanate ceramics. **Current Applied Physics**. 14(9): 1312-1317.
- Paillard, C., Bai, X., Infante, I. C., Guennou, M., Geneste, G., Alexe, M., Kreisel, J. and Dkhil, B. (2016). Photovoltaics with ferroelectrics: Current status and beyond. **Advanced Materials**. 28(26): 5153-5168.
- Palai, R., Katiyar, R., Schmid, H., Tissot, P., Clark, S., Robertson, J., Redfern, S. and Scott, J. (2007). The beta phase of multiferroic bismuth ferrite and its beta-gamma metal-insulator transition. **Physical review B**. 77(1):1-5.
- Park, J.-H., Park, J., Lee, K.-B., Koo, T.-Y., Youn, H., Ko, Y., Chung, J.-S., Hwang, J. and Jeong, S.-Y. (2007). Local strain-induced 90° domain switching in a barium titanate single crystal. **Applied Physics Letters**. 91(1): 012906.
- Pashkin, A., Rabia, K., Frank, S., Kuntscher, C., Haumont, R., Saint-Martin, R. and Kreisel, J. (2007). Pressure-induced phase transitions in the multiferroic perovskite BiFeO<sub>3</sub> studied by far-infrared micro-spectroscopy. **American Physical Society**. 79(18):184110.
- Pintilie, L. and Alexe, M. (2005). Metal-ferroelectric-metal heterostructures with Schottky contacts. I. Influence of the ferroelectric properties. **Journal of Applied Physics**. 98(12): 124103.
- Polomska, M., Kaczmarek, W. and Pająk, Z. (1974). Electric and magnetic properties of (B<sub>1-x</sub>Lax) FeO<sub>3</sub> solid solutions. **Physica Status Solidi (a)**. 23(2): 567-574.
- Pramanick, A., Prewitt, A. D., Forrester, J. S. and Jones, J. L. (2012). Domains, domain walls and defects in perovskite ferroelectric oxides: A review of present

- understanding and recent contributions. **Critical Reviews in Solid State and Materials Sciences**. 37(4): 243-275.
- Qi, X., Dho, J., Tomov, R., Blamire, M. G. and MacManus-Driscoll, J. L. (2005). Greatly reduced leakage current and conduction mechanism in aliovalent-ion-doped BiFeO<sub>3</sub>. **Applied Physics Letters**. 86(6): 062903.
- Rahaman, M. and Manalart, R. (1998). Grain boundary mobility of BaTiO<sub>3</sub> doped with aliovalent cations. **Journal of the European Ceramic Society**. 18(8): 1063-1071.
- Rai, R., Coondoo, I., Rani, R., Bdikin, I., Sharma, S. and Kholkin, A. L. (2013). Impedance spectroscopy and piezoresponse force microscopy analysis of lead-free (1-x) K<sub>0.5</sub>Na<sub>0.5</sub>NbO<sub>3</sub>-xLiNbO<sub>3</sub> ceramics. **Current Applied Physics**. 13(2): 430-440.
- Redfern, S., Walsh, J., Clark, S., Catalan, G. and Scott, J. (2009). Structural origin of the metal-insulator transition of multiferroic BiFeO<sub>3</sub>. **Arxiv Materials Science**. 1(1):1-6.
- Reichmann, A., Zankel, A., Reingruber, H., Pölt, P. and Reichmann, K. (2011). Direct observation of ferroelectric domain formation by environmental scanning electron microscopy. **Journal of the European Ceramic Society**. 31(15): 2939-2942.
- Saito, Y., Takao, H., Tani, T., Nonoyama, T., Takatori, K., Homma, T., Nagaya, T. and Nakamura, M. (2004). Lead-free piezoceramics. *Nature*. 432: 84.
- Scott, F., James F. (2009). Magnetoelectric Memories—a Disruptive Technology? **ChemPhysChem**. 10(11): 1761-1762.

- Shen, Z., Yan, H., Grüner, D., Belova, L. M., Sakamoto, Y., Hu, J., Nan, C.-W., Höche, T. and Reece, M. J. (2012). Ferroelectric ceramics with enhanced remnant polarization by ordered coalescence of nano-crystals. **Journal of Materials Chemistry**. 22(44): 23547-23552.
- Shvartsman, V. V., Kholkin, A. L., Verdier, C., Yong, Z. and Lupascu, D. C. (2005). Investigation of fatigue mechanism in ferroelectric ceramic via piezoresponse force microscopy. **Journal of the European Ceramic Society**. 25(12): 2559-2561.
- Silva, M., Souza, S., Sampaio, D., Santos, J., Fonseca, E. and Silva, R. (2016). Conductive atomic force microscopy characterization of PTCR-BaTiO<sub>3</sub> laser-sintered ceramics. **Journal of the European Ceramic Society**. 36(6): 1385-1389.
- Smolenskiĭ, G. and Kraĭnik, N. (1969). Progress in ferroelectricity. **Physics-Uspekhi**. 12(2): 271-293.
- Soergel, E. (2011). Piezoresponse force microscopy (PFM). **Journal of Physics D: Applied Physics**. 44(46): 464003.
- Tadashi, T., Kei-ichi, M. and Koichiro, S. (1991). (Bi<sup>1/2</sup> Na<sup>1/2</sup>)TiO<sub>3</sub>-BaTiO<sub>3</sub> System for Lead-Free Piezoelectric Ceramics. **Japanese Journal of Applied Physics**. 30(9S): 2236.
- Tan, Y., Zhang, J., Wu, Y., Wang, C., Koval, V., Shi, B., Ye, H., McKinnon, R., Viola, G. and Yan, H. (2015). Unfolding grain size effects in barium titanate ferroelectric ceramics. **Scientific Reports**. 5: 9953.
- Terabe, K., Nakamura, M., Takekawa, S., Kitamura, K., Higuchi, S., Gotoh, Y. and Cho, Y. (2003). Microscale to nanoscale ferroelectric domain and surface

- engineering of a near-stoichiometric LiNbO<sub>3</sub> crystal. **Applied Physics Letters**. 82(3): 433-435.
- Tybell, T., Paruch, P., Giamarchi, T. and Triscone, J. M. (2002). Domain wall creep in epitaxial ferroelectric Pb(Zr(0.2)Ti(0.08)O<sub>3</sub>) thin films. **Physical Review Letters**. 89(9): 097601.
- Uchida, H., Ueno, R., Funakubo, H. and Koda, S. (2006). Crystal structure and ferroelectric properties of rare-earth substituted Bi Fe O<sub>3</sub> thin films. **Journal of Applied Physics**. 100(1): 014106.
- Vanga, P. R., Mangalaraja, R. and Ashok, M. (2015). Effect of (Nd, Ni) co-doped on the multiferroic and photocatalytic properties of BiFeO<sub>3</sub>. **Materials Research Bulletin**. 72: 299-305.
- Walker, J., Simons, H., Alikin, D. O., Turygin, A. P., Shur, V. Y., Kholkin, A. L., Ursic, H., Bencan, A., Malic, B., Nagarajan, V. and Rojac, T. (2016). Dual strain mechanisms in a lead-free morphotropic phase boundary ferroelectric. **Scientific Reports**. 6: 19630.
- Wang, C., Jin, K.-j., Xu, Z.-t., Wang, L., Ge, C., Lu, H.-b., Guo, H.-z., He, M. and Yang, G.-z. (2011). Switchable diode effect and ferroelectric resistive switching in epitaxial BiFeO<sub>3</sub> thin films. **Applied Physics Letters**. 98(19): 192901.
- Wang, J., Neaton, J., Zheng, H., Nagarajan, V., Ogale, S., Liu, B., Viehland, D., Vaithyanathan, V., Schlom, D. and Waghmare, U. (2003). Epitaxial BiFeO<sub>3</sub> multiferroic thin film heterostructures. **Science**. 299(5613): 1719-1722.
- Wu, W., Guest, J., Horibe, Y., Park, S., Choi, T., Cheong, S.-W. and Bode, M. (2010). Polarization-modulated rectification at ferroelectric surfaces. **Physical review letters**. 104(21): 217601.

- Yan, F., Lai, M.-O., Lu, L. and Zhu, T.-J. (2010). Enhanced multiferroic properties and valence effect of Ru-doped BiFeO<sub>3</sub> thin films. **The Journal of Physical Chemistry C**. 114(15): 6994-6998.
- Yang, C.-H., Seidel, J., Kim, S., Rossen, P., Yu, P., Gajek, M., Chu, Y.-H., Martin, L. W., Holcomb, M. and He, Q. (2009). Electric modulation of conduction in multiferroic Ca-doped BiFeO<sub>3</sub> films. **Nature materials**. 8(6): 485.
- Yotburut, B., Thongbai, P., Yamwong, T. and Maensiri, S. (2017). Electrical and nonlinear current-voltage characteristics of La-doped BiFeO<sub>3</sub> ceramics. **Ceramics International**. 43(7): 5616-5627.
- Yuan, G. L. and Or, S. W. (2006). Multiferroicity in polarized single-phase Bi<sub>0.875</sub>Sm<sub>0.125</sub>FeO<sub>3</sub> ceramics. **Journal of Applied Physics**. 100(2): 024109.
- Zhao, K., Zhao, W., Zeng, H., Yu, H., Ruan, W., Xu, K. and Li, G. (2015). Tip-bias-induced domain evolution in PMN–PT transparent ceramics via piezoresponse force microscopy. **Applied Surface Science**. 337: 125-129.
- Zheng, H., Wang, J., Lofland, S. E., Ma, Z., Mohaddes-Ardabili, L., Zhao, T., Salamanca-Riba, L., Shinde, S. R., Ogale, S. B., Bai, F., Viehland, D., Jia, Y., Schlom, D. G., Wuttig, M., Roytburd, A. and Ramesh, R. (2004). Multiferroic BaTiO<sub>3</sub>-CoFe<sub>2</sub>O<sub>4</sub> Nanostructures. **Science**. 303(5658): 661-663.

## CURRICULUM VITAE

**Name** Mr. Panithan Sriboriboon

**Born** December 15<sup>th</sup>, 1993 in Sisaket, Thailand

**Citizenship** Thai

**Address** 1586/31, Tambon Maung-Tai, Amphor Maung-Sisaket, Sisaket, 33000,  
Thailand

**E-mail** Panithan.sn@gmail.com

### **Education**

2012-2016 B.Sc. (Physics), Suranaree University of Technology, Thailand

2016-present M.Sc. (Physics), Suranaree University of Technology, Thailand

### **Presentation and publication:**

**Nonkumwong, J.,** Sriboriboon, P., Kundhikanjana, W., Srisombat, L. and Ananta, S. (2018). Ferroelectric domain evolution in gold nanoparticle-modified perovskite barium titanate ceramics by piezoresponse force microscopy. *Integrated Ferroelectrics*. 187(1): 210-218.